

# Reference Climate Dataset for the Indus, Ganges, and Brahmaputra River Basins



Consortium members



ICIMOD

teri

WAGENINGEN UR  
For quality of life

FutureWater  
Onderzoek en advies, gericht op de  
duurzame toekomst van ons water

## About HI-AWARE Working Papers

This series is based on the work of the Himalayan Adaptation, Water and Resilience (HI-AWARE) consortium under the Collaborative Adaptation Research Initiative in Africa and Asia (CARIAA) with financial support from the UK Government's Department for International Development and the International Development Research Centre, Ottawa, Canada. CARIAA aims to build the resilience of vulnerable populations and their livelihoods in three climate change hot spots in Africa and Asia. The programme supports collaborative research to inform adaptation policy and practice.

HI-AWARE aims to enhance the adaptive capacities and climate resilience of the poor and vulnerable women, men, and children living in the mountains and flood plains of the Indus, Ganges, and Brahmaputra river basins. It seeks to do this through the development of robust evidence to inform people-centred and gender-inclusive climate change adaptation policies and practices for improving livelihoods.

The HI-AWARE consortium is led by the International Centre for Integrated Mountain Development (ICIMOD). The other consortium members are the Bangladesh Centre for Advanced Studies (BCAS), The Energy and Resources Institute (TERI), the Climate Change, Alternative Energy, and Water Resources Institute of the Pakistan Agricultural Research Council (CAEWRI-PARC) and Alterra-Wageningen University and Research Centre (Alterra-WUR). For more details see [www.hi-aware.org](http://www.hi-aware.org).

Titles in this series are intended to share initial findings and lessons from research studies commissioned by HI-AWARE. Papers are intended to foster exchange and dialogue within science and policy circles concerned with climate change adaptation in vulnerability hotspots. As an interim output of the HI-AWARE consortium, they have only undergone an internal review process.

Feedback is welcomed as a means to strengthen these works: some may later be revised for peer-reviewed publication.

## About the Authors

Arthur F Lutz, Physical Geographer, FutureWater, The Netherlands

Walter Immerzeel, Hydrologist, FutureWater, The Netherlands

**Corresponding Author:** Arthur F Lutz, [a.lutz@futurewater.nl](mailto:a.lutz@futurewater.nl)

## Acknowledgement

This work was carried out by the Himalayan Adaptation, Water and Resilience (HI-AWARE) consortium under the Collaborative Adaptation Research Initiative in Africa and Asia (CARIAA) with financial support from the UK Government's Department for International Development and the International Development Research Centre, Ottawa, Canada.

HI-AWARE Working Paper 2

# Reference Climate Dataset for the Indus, Ganges, and Brahmaputra River Basins

**Authors**

Arthur F Lutz

Walter Immerzeel

Himalayan Adaptation, Water and Resilience (HI-AWARE)

Kathmandu, Nepal, October 2016

**Published by****HI-AWARE Consortium Secretariat**

Himalayan Adaptation, Water and Resilience (HI-AWARE)

c/o ICIMOD

GPO Box 3226, Kathmandu, Nepal

**Copyright © 2016**

Himalayan Adaptation, Water and Resilience (HI-AWARE)

All rights reserved. Published 2016

**ISBN** ISBN 978 92 9115 420 3 (electronic)

**Production team**

Amy Sellmyer (Editor)

Punam Pradhan (Graphic designer)

Asha Kaji Thaku (Editorial assistant)

**Disclaimer:** The views expressed in this work are those of the creators and do not necessarily represent those of the UK Government's Department for International Development, the International Development Research Centre, Canada or its Board of Governors.

In addition, they are not necessarily attributable to ICIMOD and do not imply the expression of any opinion by ICIMOD concerning the legal status of any country, territory, city or area of its authority, or concerning the delimitation of its frontiers or boundaries, or the endorsement of any product.

**Creative Commons License**

This Working Paper is licensed under a Creative Commons Attribution-NonCommercial-ShareAlike 4.0 International License. Articles appearing in this publication may be freely quoted and reproduced provided that i) the source is acknowledged, ii) the material is not used for commercial purposes, and iii) any adaptations of the material are distributed under the same license.

This publication is available in electronic form at [www.hi-aware.org](http://www.hi-aware.org)

**Citation:** Lutz, AF; Immerzeel, W (2016) *Reference climate dataset for the Indus, Ganges, and Brahmaputra River Basins*. HI-AWARE Working Paper 2. Kathmandu: HI-AWARE

# Contents

<b>1. Introduction</b>	<b>1</b>
<b>2. Baseline Reference Climate Data</b>	<b>2</b>
2.1 Selection of baseline climate data	2
2.2 Upstream domain	5
2.3 Downstream domain	7
<b>3. Correction of Reference Climate Data</b>	<b>8</b>
3.1 Upstream air temperature	8
3.2 Upstream precipitation	11
3.2.1 Concept: precipitation lapse rates	11
3.2.2 Region-wide glacier mass balance	12
3.2.3 Model implementation and uncertainty analysis	14
3.3 Downstream climate	15
<b>4. Corrected Reference Climate Data</b>	<b>16</b>
4.1 Upstream dataset	16
4.1.1 Air temperature	16
4.1.2 Precipitation	17
4.2 Total IGB domain	19
4.2.1 Air temperature	19
4.2.2 Precipitation	21
4.2.3 Reference evapotranspiration	22
4.3 Subregional summaries and trends in time	23
<b>5. Dataset Metadata</b>	<b>25</b>
5.1 Upstream IGB dataset	25
5.2 Total IGB dataset	25
<b>Reference</b>	<b>26</b>



# 1. Introduction

High-altitude climates are particularly uncertain, and commonly used climate datasets are grossly inaccurate at high altitudes. Therefore, a novel reference climate dataset covering the Indus, Ganges, and Brahmaputra (IGB) river basins has been constructed with a particular focus on improved representation of high-altitude precipitation.

This document describes the construction of a historical climate dataset for the IGB river basins, which has been constructed for widespread use in the HI-AWARE project. The dataset covers the period from 1 January 1981 to 31 December 2010 with a daily time step and covers the IGB river basins at 10x10 km spatial resolution. Additionally, the upstream parts of the basins are covered at 5x5 km spatial resolution in a separate dataset to account for the larger variability in mountainous terrain. The methods used to generate the dataset have been discussed and the contents of the dataset have been illustrated in this document.

Recently, a method was developed that uses the presumed glacier mass balance to infer high-altitude precipitation; based on the size and mass balance of a glacier, it is possible to estimate the amount of precipitation that is required to sustain this mass balance [*Immerzeel et al.* 2012, 2015]. This approach was adapted and extended to the upstream parts of the IGB basins. For the downstream areas, which are less affected by steep topography, straightforward geostatistical interpolation techniques were used. These corrections resulted in a high-quality, high-resolution historical reference dataset spanning over 30 years. The corrections of the upstream and downstream domains were done separately, and the resulting products were merged and stored as NetCDF files, which are available for all consortium partners. At the end of the document, the technical metadata of the dataset are listed.

# 2. Baseline Reference Climate Data

## 2.1 Selection of baseline climate data

Understanding the spatial and temporal variability of precipitation in mountainous areas remains a key challenge. Point measurements are often not sufficient to capture the strong gradients in the multiple local factors that determine the distribution of precipitation. Based on observations, climatologists have created numerous gridded datasets. Since many of the existing gridded data products include precipitation and temperature at near-surface level, they can be used to overcome data gaps in observations.

Several distinctions, in two groups, can be made among gridded datasets for temperature and precipitation: (i) datasets created using advanced geo-statistical interpolation techniques based on station observations, (ii) datasets based on blending of climate model output and observations (often referred to as reanalysis products), and (iii) datasets based on satellite observations (remote sensing). Apart from differences in the underlying methodology (interpolation of observations or reanalysis), the main differences that are found among such datasets are the spatial resolution, temporal resolution, and the time span covered.

A thorough comparison on the performance of existing gridded products for the Hindu Kush Himalayan (HKH) region [Palazzi *et al.*, 2013] highlights the striking differences between the different products. All analysed products are subject to limited spatial resolution. They are mostly suitable for large-scale continental studies. However, in analysing climate variations at smaller scales and in orographically complex regions, such as the IGB, they lack accuracy.

Researchers who compared the performance of the Tropical Rainfall Measuring Mission (TRMM) and the Asian Precipitation - Highly - Resolved Observational Data Integration Towards Evaluation (APHRODITE) all over Nepal have concluded that the latter is the more accurate dataset [Duncan and Biggs, 2012]. Other researchers have also concluded that there is large variability in performance between different gridded products by comparing them for multiple transects crossing the Himalayan ranges [Andermann *et al.*, 2011]. They have agreed that APHRODITE, based solely on the ground station data, gives the best precipitation estimates. However, they have also mentioned that the lack of a sufficient number of stations at high elevations limits the accuracy of this dataset. Similarly, a study on the Upper Indus basin has also shown that high-altitude precipitation is strongly underestimated in APHRODITE [Lutz *et al.*, 2014]. Immerzeel *et al.* [2015], on the other hand, compared four precipitation products for the Upper Indus basin and validated them with the observed river discharge. According to their analysis, ERA-Interim provides the best estimate of precipitation in terms of annual totals. However, the relatively coarse resolution limits its usability.

In 2014, the High-Asia Refined analysis (HAR) was released [Maussion *et al.*, 2014]. HAR is based on the Weather Research and Forecasting (WRF) model which runs with an hourly time step, bounded daily to the ERA-Interim dataset. Although the product has a high spatial (10 km) and temporal (1 h) resolutions, it covers a relatively short time range (2000–2012), and does not cover the entire IGB, since the western part of the upper Indus basin is not included.

The Watch Forcing Data ERA-Interim (WFDEI) dataset [Weedon *et al.*, 2014], is based on the WATCH methodology [Weedon *et al.*, 2011], integrated with the ERA-Interim dataset [Dee *et al.*, 2011]. Precipitation in the WFDEI dataset is bias-corrected for bias using either the Global Precipitation Climatology Centre (GPCC) dataset [Schneider *et al.*, 2013] dataset or the Climate Research Unit (CRU) dataset [Harris *et al.*, 2013].

Because ERA-Interim showed the most realistic precipitation totals as mentioned above, the decision was made to use an ERA-Interim-based dataset as a basis. A comparison of the ERA-Interim based WFDEI dataset to the raw ERA-Interim dataset showed that WFDEI has a higher spatial resolution than ERA-Interim and that WFDEI precipitation

data that is bias-corrected using GPCC [Schneider *et al.*, 2013] shows more realistic spatial patterns as a result of the correction with station data (Figure 1). It is desirable to use temperature data from the same dataset to ensure physical consistency between the two climatic variables (e.g. lower temperatures on rainy days), thus the WFDEI temperature data is also used as a basis.

Figure 1: **Average annual precipitation sum 1998-2007 according to WFDEI corrected with CRU (upper panel), WFDEI corrected with GPCC (middle panel), and raw ERA-Interim (lower panel). Resolutions are the products' nominal resolutions.**

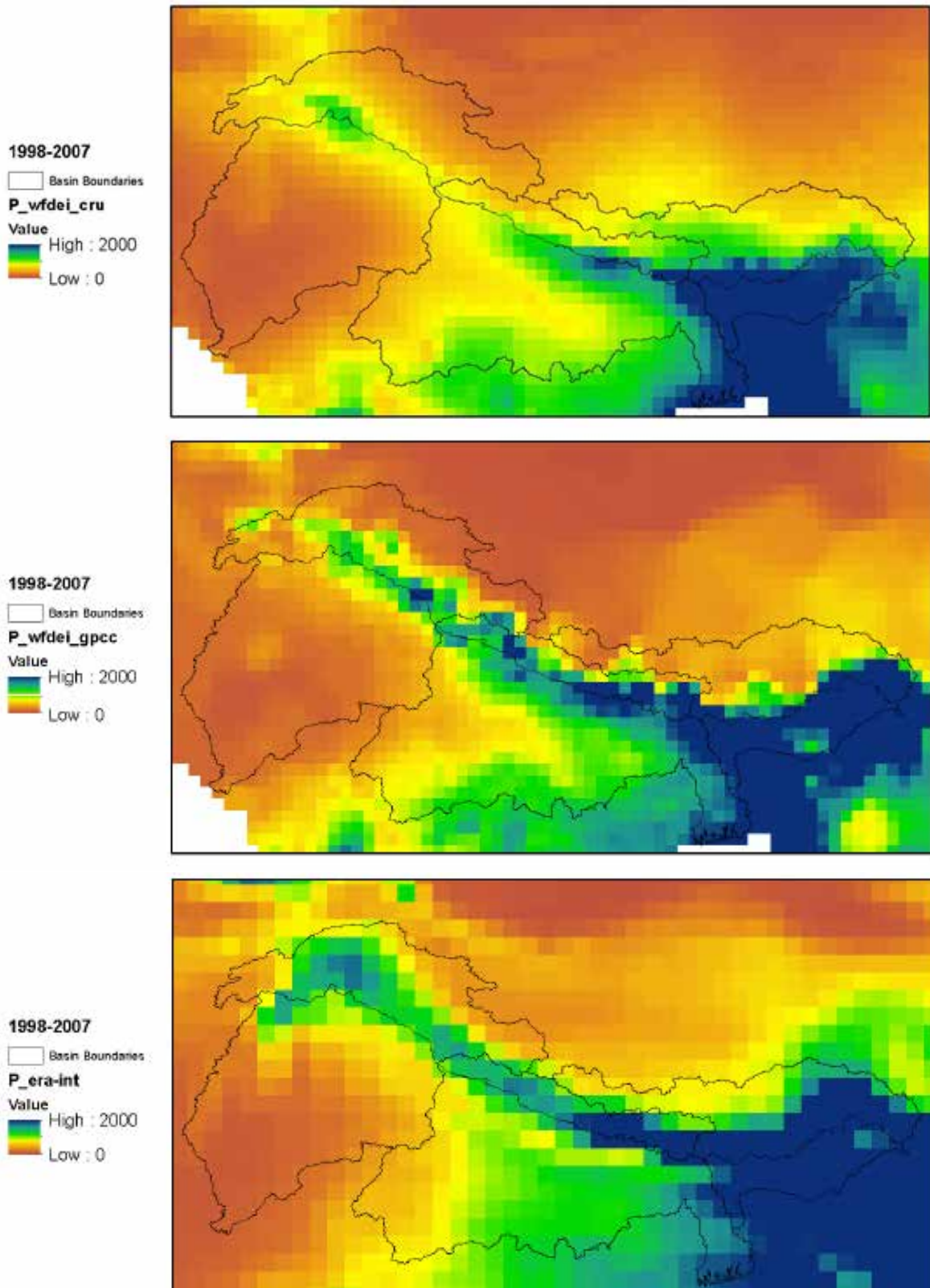


**Table 1: Average annual precipitation sum 1998–2007 for the upper Indus basin (UIB), upper Ganges basin (UGB), and upper Brahmaputra basin (UBB).**

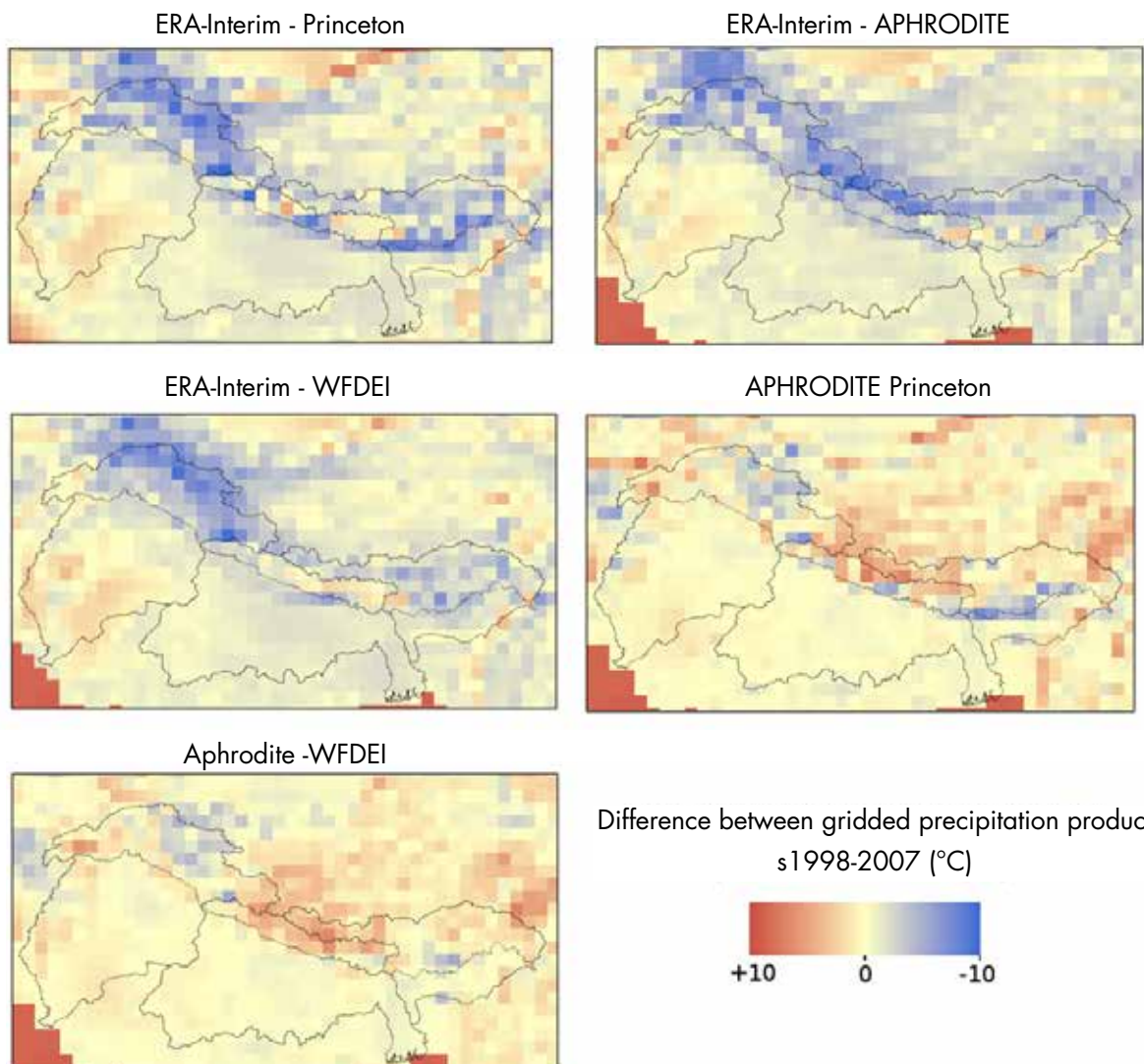
Product	P upper basins 1998-2007 (mm/yr)	P UIB 1998-2007 (mm/yr)	P UGB 1998-2007 (mm/yr)	P UBB 1998-2007 (mm/yr)
WFDEI CRU	809	565	1004	1043
WFDEI GPCC	925	611	1488	1117
ERA-INT	1441	967	1704	1888

Figure 2 indicates that the differences between the different air temperature datasets are very large. They are in the order of several degrees Celsius, with maximum differences around 10 degrees Celsius. Averaged over the upstream basins, the differences between the different datasets are also significant (Table 2).

**Table 2: Mean air temperature 1998–2007 for the upstream GB according to different gridded air temperature products.**

Product	Mean T upstream IGB 1998-2007 (°C)
ERA-Interim	1.38
Aphrodite	5.34
Princeton	4.93
WFDEI	4.42

**Figure 2: Comparison of different gridded air temperature products.**



## 2.2 Upstream domain

The raw daily mean air temperature from the WFDEI dataset is spatially interpolated from a  $0.5^\circ \times 0.5^\circ$  ( $\sim 50 \times 50$  km) to 1x1 km spatial resolution using a cubic spline interpolation and subsequently downscaled using a digital elevation model (DEM) at 1x1 km resolution (Figure 3, upper left) and vertical temperature lapse rates. Elevation differences (Figure 3, lower panel) between the DEM at 1x1 km resolution and the DEM used in WFDEI at  $0.5^\circ \times 0.5^\circ$  resolution (Figure 3, upper right) determine the vertical distance over which the air temperature data is lapsed.

Temperature lapse rates vary locally, as under high and dry conditions, the lapse rates are generally more steep than for under humid conditions [Kattel *et al.*, 2012; Immerzeel *et al.*, 2014]. Therefore, the vertical lapse rate is determined locally at a monthly time scale. For this lapse rate derivation, lapse rates are determined at the  $0.5^\circ \times 0.5^\circ$  grid cell level by doing a neighbourhood operation for the grid cell under consideration and its eight neighbouring grid cells. A linear temperature-elevation relation is fitted using the nine pairs of grid cell elevation and air temperature. This is done at a daily time step. Outliers are removed from the daily grids that are constructed in this way. Values outside the range of  $\mu \pm 2\delta$  are considered outliers. The resulting grid is spatially smoothed by averaging values over a  $3 \times 3$  grid cells moving window. Daily grids are averaged over a month and the resulting monthly grids are used to downscale daily air temperature as:

$$T_{DS,d} = T_{WFDEI,d} + (DEM_{1km} - DEM_{WFDEI}) * \gamma_m$$

where  $T_{DS,d}$  is the daily downscaled air temperature,  $T_{WFDEI,d}$  is the daily temperature in WFDEI, and  $\gamma_m$  is the monthly spatial grid with the vertical temperature lapse rate.

Figure 3: High-resolution 1x1 km DEM (upper left), WFDEI nominal  $0.5 \times 0.5$  DEM (upper right), and vertical difference between the two DEMs at 1x1 km resolution (lower panel).

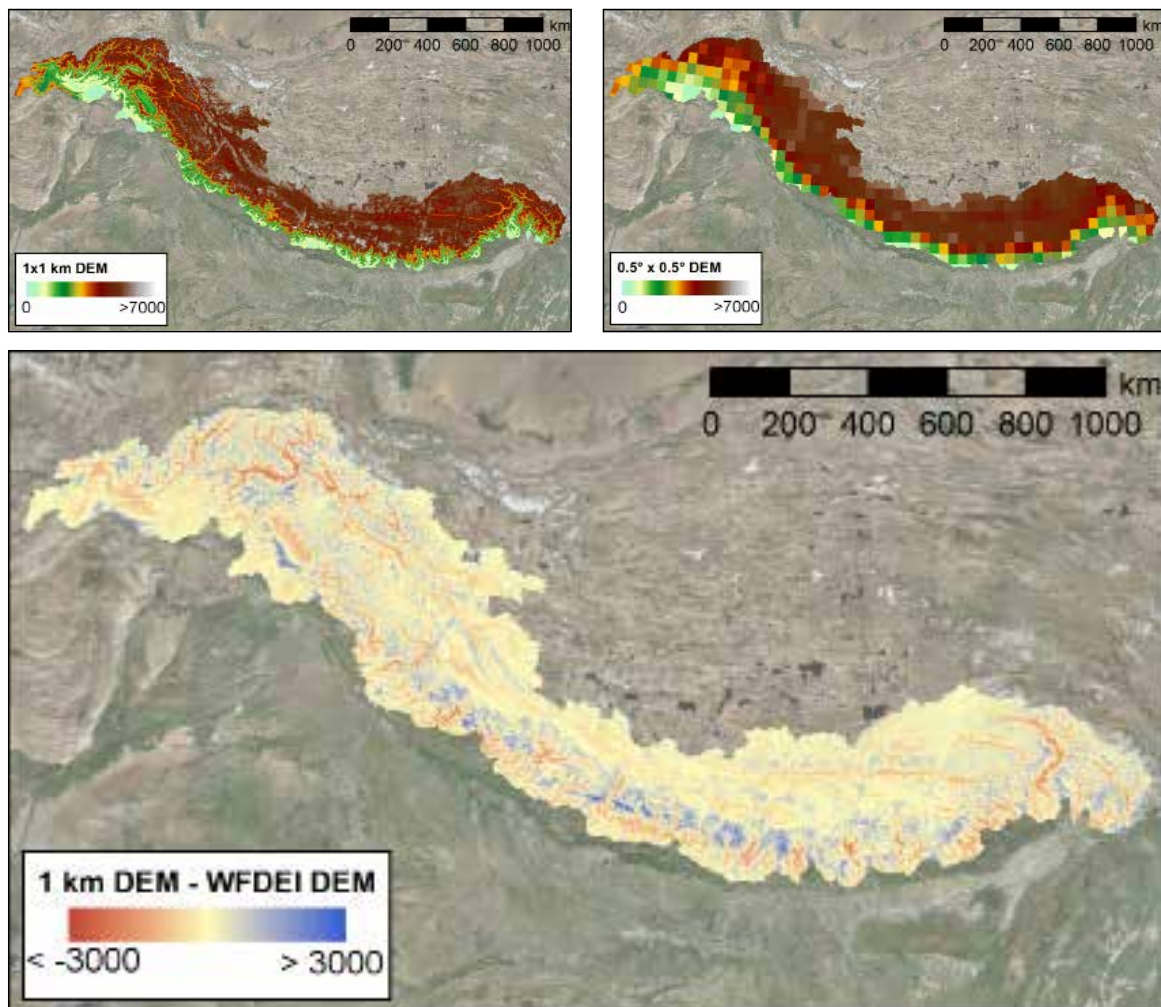
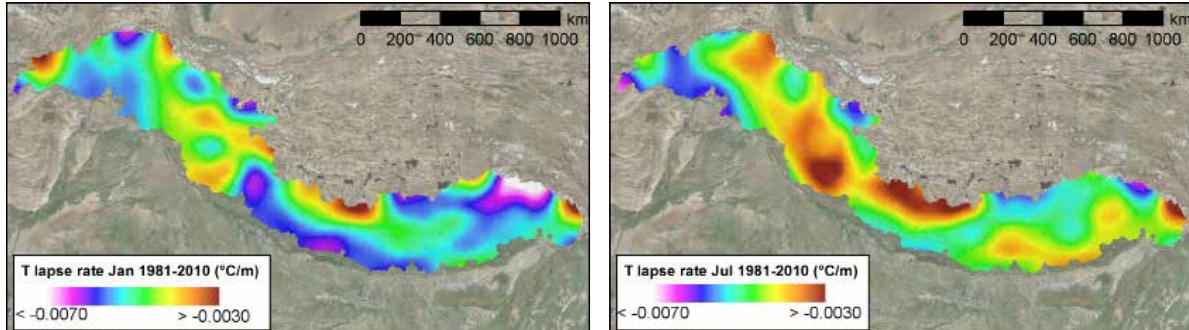


Figure 4 shows the average vertical temperature lapse rates for January and December. The differences are generally as expected, with steeper lapse rates observed during the dryer month of January and shallower lapse rates during July, when the monsoon occurs.

Figure 4: **Average vertical temperature lapse rate for January (left) and July (right) 1981-2010.**



Maximum and minimum air temperatures are pre-processed in a very similar way. Since these data are not readily available in the WFDEI dataset at a daily time step, they are derived from the three-hourly data, with the daily maximum air temperature being the maximum value among the eight three-hourly values during the day and the minimum air temperature being the minimum value among the eight three-hourly values. These temperature fields are downscaled using the same vertical lapse rates as that are used for the average air temperature. Although, in reality, the lapse rates may actually be different for maximum, minimum, and average air temperatures, the same lapse rates are used for each of these variables to ensure data consistency. Otherwise, a situation can occur where the average air temperature becomes higher than the maximum air temperature or lower than the minimum air temperature. Similarly, the maximum air temperature could become lower than the minimum air temperature.

Precipitation data in WFDEI is only available differentiated as rain and snow. Therefore, both fields are summed during preprocessing. Subsequently, the data are interpolated from  $0.5^\circ \times 0.5^\circ$  to  $1 \times 1$  km by a cubic spline interpolation.

Figure 5: **Uncorrected mean air temperature 1981-2010 (left) and uncorrected annual precipitation 1981-2010 (right) at 1x1 km resolution.**

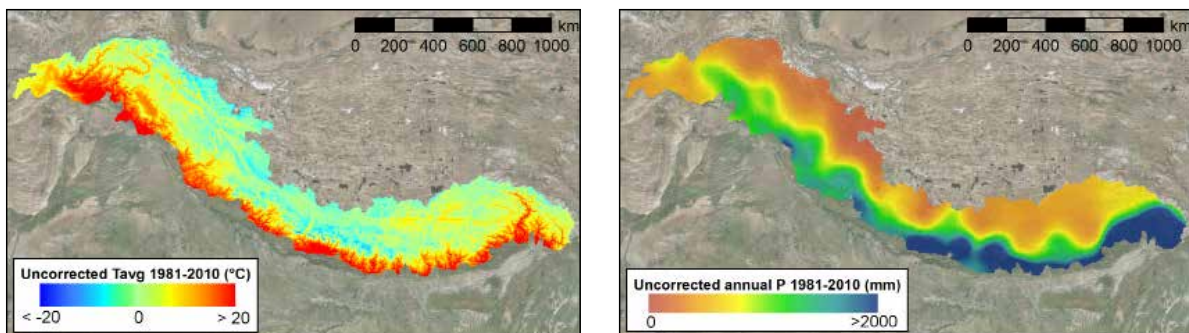


Table 3: **Basin-averaged air temperature and precipitation 1981-2010 (uncorrected data).**

	Upper Indus	Upper Ganges	Upper Brahmaputra
Mean T 1981-2010 (°C)	4.39	6.31	3.59
Mean annual P 1981-2010 (mm)	617	1497	1119

## 2.3 Downstream domain

The Air air temperature for the downstream domain is downscaled from a  $0.5^\circ \times 0.5^\circ$  ( $\sim 50 \times 50$  km) resolution to a  $10 \times 10$  km resolution using a DEM at a  $10 \times 10$  km resolution in a way similar to that used for the upstream domain.

In

this case, the vertical lapse rates are not derived from the data itself, but a fixed lapse rate of  $-0.0065^\circ\text{C m}^{-1}$  is assumed, close to the mean value between the dry and saturated adiabatic lapse rates [Immerzeel *et al.*, 2012].

Precipitation data are interpolated to a  $10 \times 10$  km resolution using a cubic spline interpolation, similar to that used for the upstream domain.

Figure 6: Mean air temperature (left) and annual precipitation sum (right) 1981-2010 for the IGB domain.

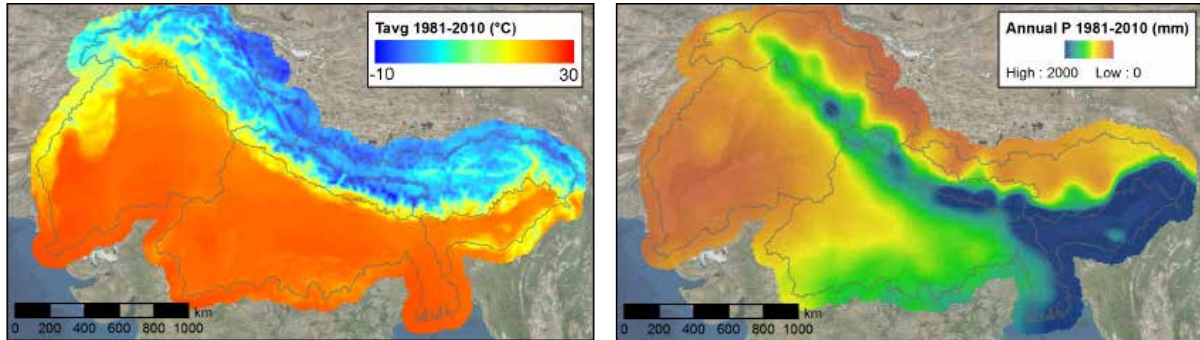


Table 4: Mean air temperature and mean precipitation (1981–2010) per basin.

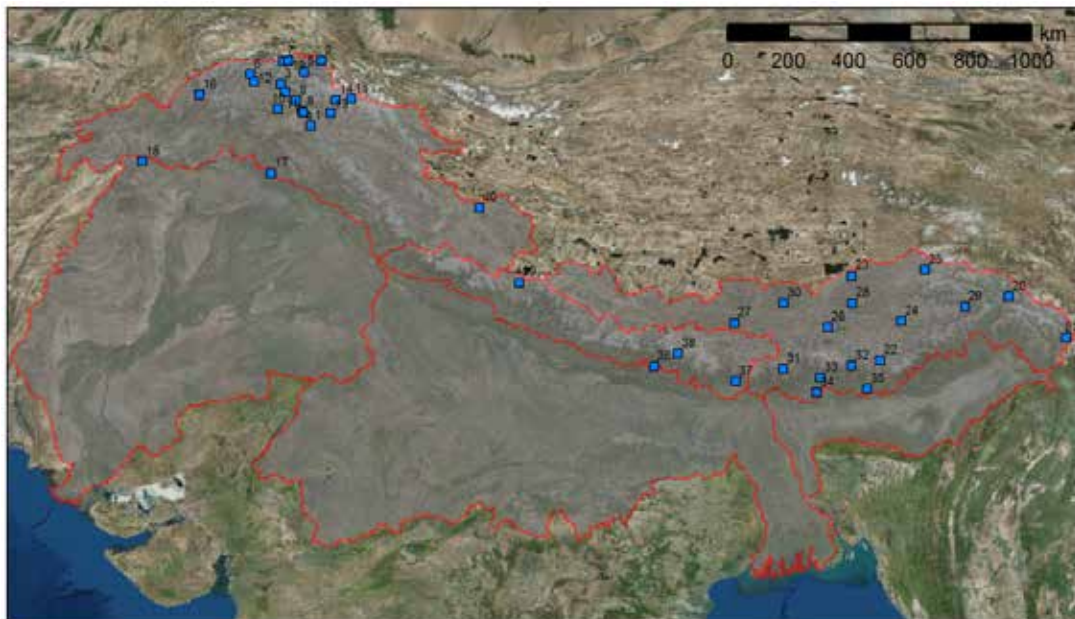
	Mean T 1981-2010 ( $^\circ\text{C}$ )	Annual P 1981-2010 (mm)
Upper Indus	4.48	654
Lower Indus	23.97	372
Upper Ganges	4.96	1460
Lower Ganges	25.19	1139
Upper Brahmaputra	2.80	1051
Lower Brahmaputra	22.56	2842

# 3. Correction of Reference Climate Data

## 3.1 Upstream air temperature

The air temperature data in the upstream domain is bias-corrected with data from station observations. Station observations in the upstream parts of the IGB basins are sparse. Figure 7 and Table 5 list the stations and station metadata, including the record length, as used in this project. As evident from the map, the stations are very unequally distributed over the basin and mostly located in the valleys. As can be seen in the table, eight out of forty 40 stations are located above 4000 m a.s.l., with the highest being located at an elevation of 4730 m a.s.l.. In addition, many stations have only rather short records available.

Figure 7: **Locations of meteorological stations in the upper IGB basins.**



In a preceding previous project that was implemented by FutureWater for ICIMOD, station temperature data were corrected using a linear relationship that was found between the temperature bias in the APHRODITE dataset and elevation in the upper Indus basin [Lutz *et al.*, 2014; Immerzeel *et al.*, 2015]. In this case, by using WFDEI for the upstream IGB basins, no such correlation could be established (Figure 8). Therefore, the average biases at the stations' locations were interpolated spatially to generate a spatial correction grid, which was applied to the uncorrected temperature fields. An additional bias-correction was made by using the degree-day glacier melt simulation component in Spatial Process in Hydrology (SPHY) [Terink *et al.*, 2015] to simulate the distributed amount of melt over the glaciers using the temperature fields that are bias-corrected to the station observations. These temperature fields are corrected downwards (to cooler temperatures) for unrealistically high amounts of melt. This is done by assuming a maximum annual ablation rate of  $1.35 \text{ m we yr}^{-1}$  based on findings in scientific literature and field data from the Khumbu area [Immerzeel *et al.*, 2011; Ragettli *et al.*, 2015; Wagon, personal communication]. The uncertainty in this assumption is taken into account in a Monte Carlo analysis of 100 runs with the uncertainty in the maximum annual ablation rate assumed to be Gaussian distributed with a mean value  $1.35 \text{ m we yr}^{-1}$  and 0.50 m a standard deviation of 0.50 m.

Table 5: Meteorological ground station records in the upper IGB used in HIAWARE.

ID	Name	Source	Lon (dd)	Lat (dd)	Elevation (masl)	Start date	End date
1	Burzil	WAPDA	75.088	34.911	4030	01/01/2000	31/12/2008
2	Khunjerab	WAPDA	75.400	36.850	4730	01/01/2000	31/12/2008
3	Naltar	WAPDA	74.189	36.158	2810	01/01/2000	31/12/2008
4	Rama	WAPDA	74.817	35.367	3000	01/01/2000	31/12/2008
5	Rattu	WAPDA	74.871	36.515	2570	01/01/2000	31/12/2008
6	Yasin	WAPDA	73.300	36.450	3150	01/01/2000	31/12/2008
7	Ziarat	WAPDA	74.276	36.836	3669	01/01/2000	31/12/2008
8	Astore	PMD	74.857	35.329	2168	01/01/2000	31/12/2005
9	Bunji	PMD	74.633	35.667	1470	01/01/2000	31/12/2005
10	Chilas	PMD	74.100	35.417	1251	01/01/2000	31/12/2005
11	Gilgit	PMD	74.333	35.917	1459	01/01/2000	31/12/2005
12	Gupis	PMD	73.400	36.230	2156	01/01/2000	31/12/2005
13	Skardu	PMD	75.680	35.300	2210	01/01/2000	31/12/2005
14	Askole	PMD	75.815	35.681	3015	10/08/2005	31/12/2007
15	Urdukas	PMD	76.286	35.728	3927	06/17/2004	31/12/2007
16	Chitral	PMD	71.780	35.839	1500	01/01/2000	01/01/2005
17	Kotli	PMD	73.900	33.520	2017	01/01/2000	01/01/2005
18	Parachinar	PMD	70.083	33.867	1726	01/01/2000	01/01/2005
19	Khunjerab	Winiger/ICIMOD	74.417	36.850	4700	01/01/2000	12/31/2012
20	Bomi	ICIMOD	95.760	29.860	2736	01/01/2000	12/31/2006
21	Chayu	ICIMOD	97.460	28.650	2327.6	01/01/2000	12/31/2006
22	Cuona	ICIMOD	91.950	27.980	4280	01/01/2000	12/31/2006
23	Dangxiong	ICIMOD	91.100	30.480	4200	01/01/2000	12/31/2006
24	Jiacha	ICIMOD	92.580	29.150	3260	01/01/2000	12/31/2006
25	Jiali	ICIMOD	93.280	30.660	4488.8	01/01/2000	12/31/2006
26	Langkazi	ICIMOD	90.400	28.960	4431.7	01/01/2000	12/31/2006
27	Lazi	ICIMOD	87.630	29.080	4000	01/01/2000	12/30/2005
28	Lhasa	ICIMOD	91.130	29.670	3648.7	01/01/2000	12/31/2006
29	Linzhi	ICIMOD	94.470	29.570	3000	01/01/2000	12/31/2006
30	Namulin	ICIMOD	89.100	29.680	4000	01/01/2000	12/31/2006
31	Pali	ICIMOD	89.080	27.730	4300	01/01/2000	12/31/2006
32	Dungkhar	ICIMOD	91.100	27.820	2010	01/01/2000	12/31/2006
33	Phobjekha	ICIMOD	90.180	27.470	2860	01/01/2000	12/31/2006
34	Sunkosh	ICIMOD	90.070	27.020	410	01/01/2000	12/31/2006
35	Wamrong	ICIMOD	91.570	27.130	2180	01/01/2000	12/31/2006
36	Kakani	ICIMOD	85.250	27.800	2064	01/01/2000	12/31/2009
37	Taplejung	ICIMOD	87.667	27.350	1732	01/01/2000	12/31/2010
38	Nielamu	ICIMOD	85.960	28.180	3310	01/01/2000	12/31/2006
39	Pulan	ICIMOD	81.250	30.280	3900	01/01/2000	12/31/2006
40	Shiquanhe	ICIMOD	80.080	32.500	4278	01/01/2000	12/31/2006

Figure 8: Average monthly bias between uncorrected temperature data and stations (1981-2010) plotted versus station elevation.

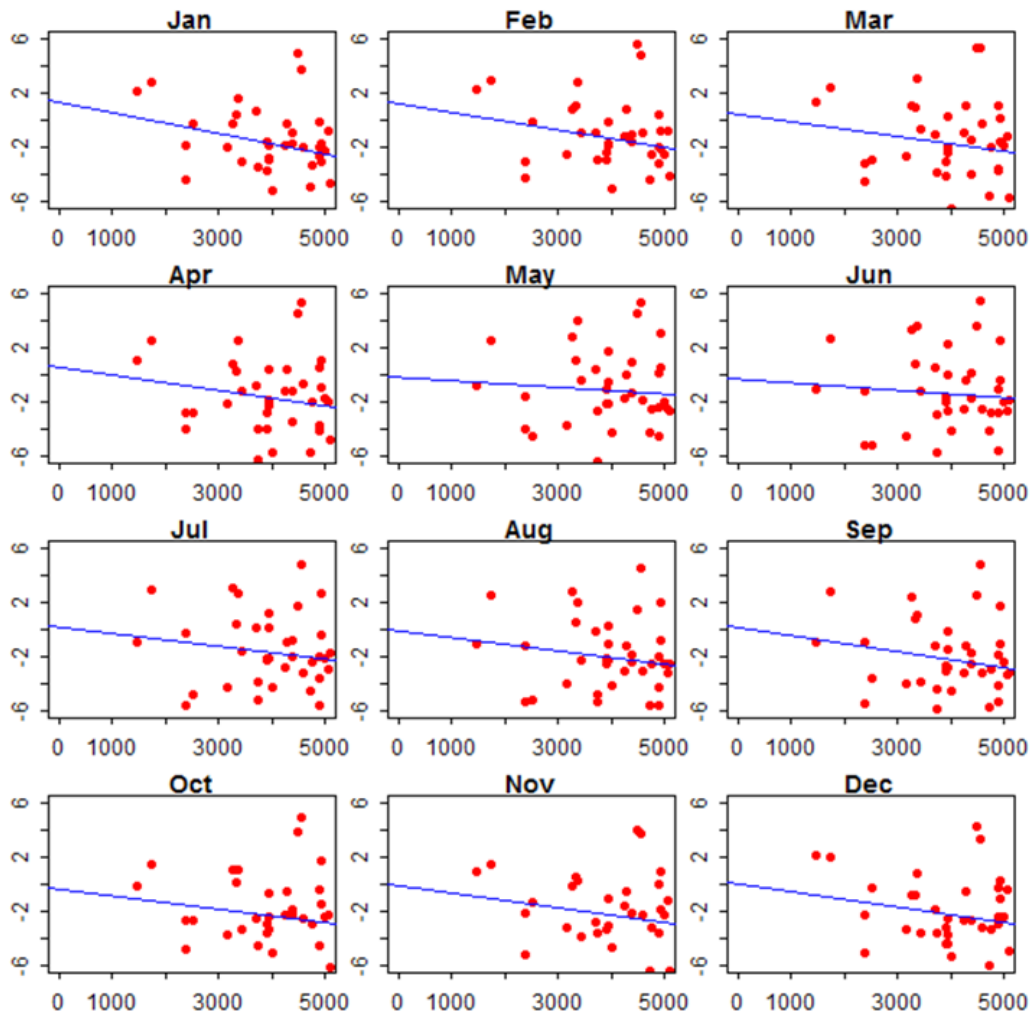
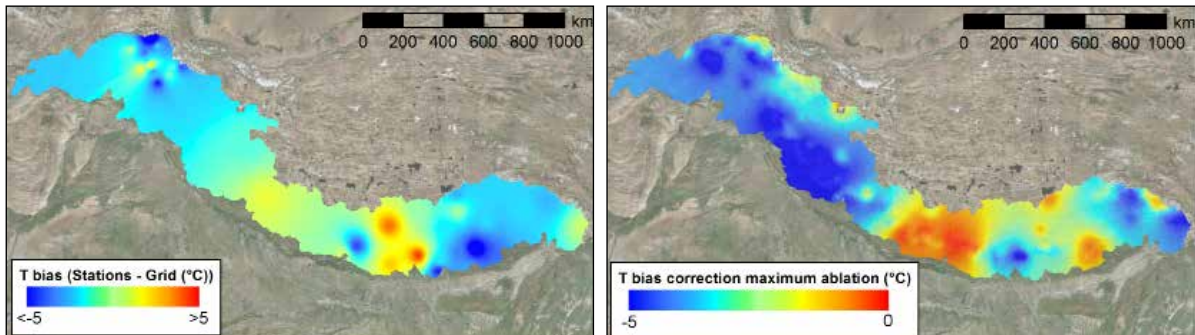


Figure 9: Spatially interpolated bias between station observations and uncorrected air temperature grids 1981-2010 (left), and spatially interpolated bias derived from maximum ablation rate over glaciers 2000-2010.



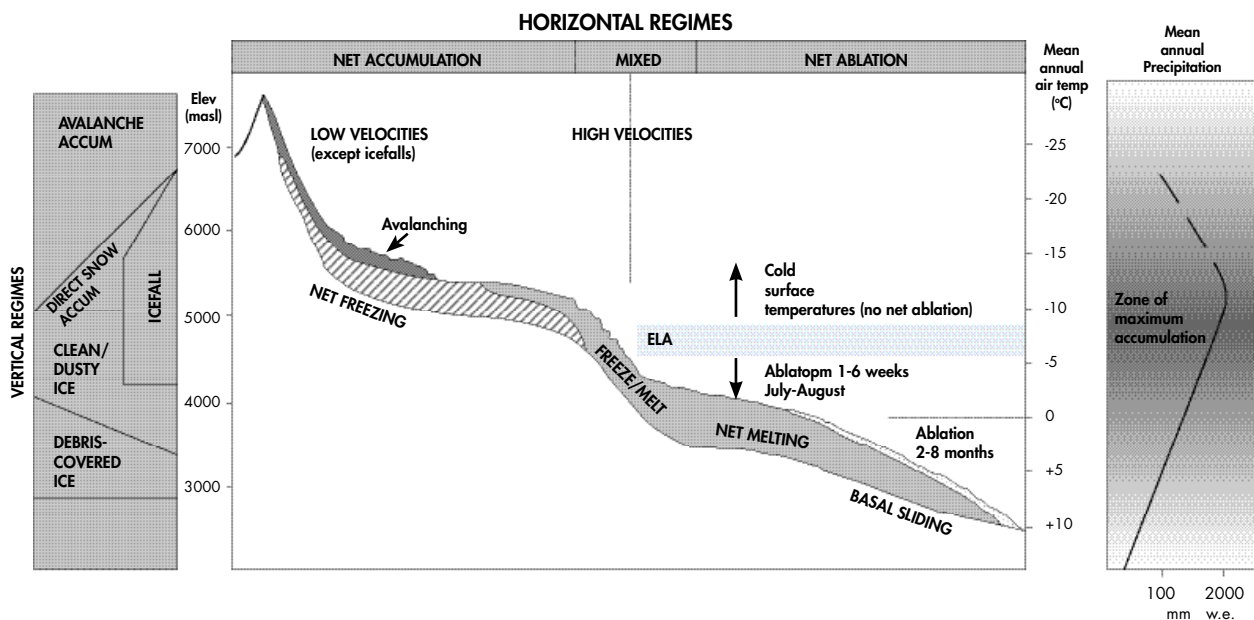
## 3.2 Upstream precipitation

### 3.2.1 Concept: precipitation lapse rates

The precipitation data is corrected using observed glacier mass balance data, according to the methodology developed in [Immerzeel *et al.*, [2012, 2015]. Based on geodetic measurements of glacier mass balance [Gardelle *et al.*, 2012, 2013], precipitation gradients are calculated to improve and downscale the uncorrected WFDEI precipitation fields.

Since the amounts of precipitation in the ground station data and gridded products are underestimated, it is very likely that the precipitation necessary to supply the observed amount of discharged water is occurring at high altitudes. Research in this area [“Batura Investigations Group,” 1979; Hewitt, 2005, 2007, 2011; Winiger *et al.*, 2005] suggests that precipitation increases between 5000 to 6000 m a.s.l., where it is at its maximum, and decreases at higher altitudes (Figure 10, right panel).

Figure 10: **Conceptual model of vertical and horizontal meteorological and cryospheric regimes in the Karakoram (Hewitt 2007).**



In the construction of an improved gridded meteorological dataset for the upper IGB basins, we implement this conceptual model to infer vertical precipitation lapse rates based on a linear increase in precipitation from a certain reference elevation (HREF) up to an elevation of maximum precipitation (HMAX) and decreasing linearly at higher altitudes with the same lapse rate [Immerzeel *et al.*, 2012, 2015].

In summary, the methodology to improve the data for precipitation is as follows:

Observed geodetic mass balance data is used to construct a spatial mass balance grid covering the upstream IGB basins

- Using the downscaled and bias-corrected temperature fields (section 3.1), a distributed ablation model is applied to the glaciers in the IGB.
- Local precipitation lapse rates are derived at the glacier level to correct uncorrected precipitation data such that the observed mass balance can be sustained taking into account the simulated ablation.
- Local precipitation lapse rates are spatially interpolated to correct precipitation for the entire upstream IGB.
- The corrected precipitation is aggregated from 1x1 km resolution to 5x5 km resolution.

We assume that precipitation increases linearly with elevation up to an elevation with maximum precipitation and decreases with the same lapse rate above that elevation:

$$P_{COR}(x, y) = P_{WFDEI}(x, y) \cdot (1 + ((\square(x, y) - \square_{ref}(x, y)) \cdot \gamma \cdot 0.01))$$

for  $h < H_{MAX}$ , and:

$$P_{COR}(x, y) = P_{WFDEI}(x, y) \cdot \left\{ 1 + \left( \left( (\square_{MAX} - \square_{ref}(x, y)) + (\square_{MAX} - \square(x, y)) \right) \cdot \gamma \cdot 0.01 \right) \right\}$$

for  $h \geq H_{MAX}$

where  $P_{COR}$  is the corrected precipitation,  $P_{WFDEI}$  is the precipitation according to WFDEI,  $h_{ref}$  is a reference elevation from which the precipitation gradients occur,  $h$  is the elevation for the grid cell, and  $\gamma$  is the precipitation gradient ( $\% m^{-1}$ ).

### 3.2.2 Region-wide glacier mass balance

To calculate the precipitation gradients for individual glacier systems, we use geodetic mass balance data for eight sites in the HKH region [Gardelle et al., 2012, 2013] (Figure 11). From these sites, we select all glacier systems that have an area greater than 5 km<sup>2</sup>, which constitutes 346 individual systems in the eight regions in the IGB (Table 6). Glaciers that are not completely covered by a geodetic mass balance grid are also removed. For each study site, Gardelle et al. [2013] used the Shuttle Radar Topographic Mission (SRTM) version 4 DEM, acquired in mid-February 2000, as the reference topography. The elevation differences between the SRTM DEM and SPOT DEMs acquired between 2008 and 2011 depending on the study site, have been analysed at the grid-cell level and corrected for several biases except for seasonality (see [Gardelle et al., 2013] for details). The elevation differences are converted to ice mass changes (meters water equivalent) using a recommended density of 850 kg m<sup>-3</sup> [Huss, 2013]. Using glacier outlines from the ICIMOD glacier inventory [Bajracharya and Shrestha, 2011], the observed mass balance per glacier is calculated from the geodetic mass balance grids. Within each region, outliers are removed. Glaciers with average geodetic mass balance values deviating by two or more standard deviations from the regional mean are considered outliers.

Figure 11: Sites in the HKH region where geodetic mass balance data has have been analysed by [Gardelle et al., 2013]. Figure source: [Gardelle et al., 2013].

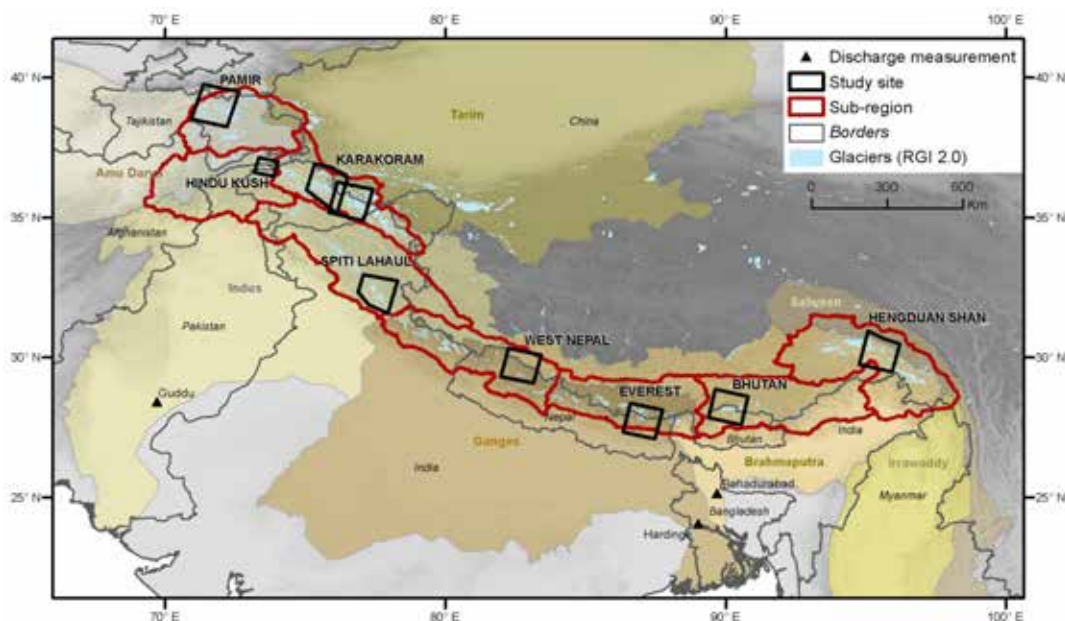
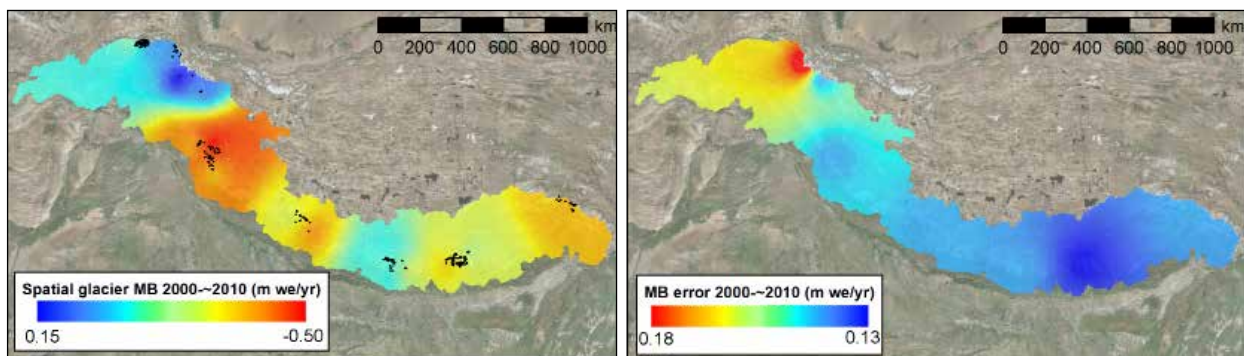


**Table 6: Properties of sites in the HKH region where geodetic mass balance data has been analysed by Gardelle et al. [2013].**

Site	Name	Date of SPOT5 DEM	No. of glaciers > 5 km <sup>2</sup>	Average MB (m we yr <sup>-1</sup> ) [Gardelle et al., 2013]	MB error (m we yr <sup>-1</sup> ) [Gardelle et al., 2013]	$\sigma$ between glaciers (MB error * $\sqrt{n}$ )
1	Hindu Kush	17-21 Oct 2008	24	-0.12	0.16	0.784
2	Karakoram West	3 Dec 2008	52	0.09	0.18	1.298
3	Karakoram East	31 Oct 2010	37	0.11	0.14	0.856
4	Spiti Lahaul	20 Oct 2011	59	-0.45	0.14	1.075
5	West Nepal	3 Jan 2011	27	-0.32	0.14	0.727
6	Everest	4 Jan 2011	43	-0.26	0.14	0.918
7	Bhutan	20 Dec 2010	45	-0.22	0.13	0.872
8	Hengduan Shan	24 Nov 2011	59	-0.33	0.14	1.075

The glacier mass balance per glacier is spatially interpolated by an inverse distance weighted interpolation and additional smoothing using a moving window averaging to obtain a spatial mass balance grid covering the entire IGB (Figure 12). Subsequently, the glacier mass balance for glaciers in the IGB basins that are not included in one of the eight regions for which the geodetic glacier mass balance has been determined is taken from this spatially interpolated grid. The uncertainty in the mass balance data is provided for each region by [Gardelle et al., [2013]. This error is spatially interpolated to get the error of the mass balance at interpolated locations (Figure 12). This error is taken into account in a Monte Carlo uncertainty analysis.

**Figure 12: Spatially interpolated grid of glacier mass balance interpolated from glaciers indicated with black dots (left). Interpolated error in mass balance (right).**



A glacier's mass balance is determined by the amount of accumulation and the amount of ablation:

$$\Delta M = C - A$$

where C is the accumulation and A is the ablation. For each of the glacier systems, the ablation can be determined using the distributed degree day melt model in SPHY at 1x1 km resolution forced with the corrected gridded temperature fields. Calculating the glacier accumulation is a bit more complex, since the accumulation area of a glacier is often not entirely included in the glacier outlines of a glacier inventory. Especially in the HKH region, the glacier accumulation consists, to a great extent, of large part, of snow fed to the glacier surface by avalanching. To include this, we assume the accumulation area of a glacier system to include the grid cells covered by the glacier outline from the glacier inventory and, in addition, the adjacent grid cells that have their "drain" direction to the glacier surface and have a slope steeper than 0.20 m m<sup>-1</sup>. This slope threshold is estimated from the slope distribution of the glacierised area in the UIB. The uncertainty in this assumption is included in a Monte Carlo uncertainty analysis.

### 3.2.3 Model implementation and uncertainty analysis

The model is implemented at a 1x1 km spatial resolution, running from February 2000, which is the acquisition date of the SRTM DEM, until 31 December 2010, which is the last day included in the reference climate dataset. Depending on the acquisition date of the SPOT5 DEM, the mass balance state on that date is used to calculate the average simulated mass balance for each glacier. One hundred realizations are run, in which the model parameters are varied according to their uncertainties (Table 7). For each realisation, the model is run twice, with fixed precipitation gradients of 0.3 and 0.6 % m<sup>-1</sup>. The precipitation gradient is then optimised by a linear regression through these two precipitation gradient values and the associated simulated mass balances to find the precipitation gradient which that is required to simulate the observed glacier mass balance. The resulting precipitation gradients over the individual glaciers are spatially interpolated by a kriging operation.

Figure 13 shows the corrected mean annual precipitation from 2000-2010 resulting from the 100 realisations. The strongest corrections are made in the eastern part of the Karakoram (Figure 14, lower left and lower right) with up to seven times more precipitation in the corrected product compared to the original WFDEI. The largest uncertainties are present in the southern ranges of the Himalayas in the Brahmaputra basin (Figure 14, upper right).

The correction grid (Figure 14, lower left) is subsequently multiplied with the uncorrected daily precipitation grids from 1981-2010, which are then aggregated to 5x5 km to be used as model forcing for the upstream SPHY model at a later stage of the project.

Figure 13: **Corrected mean annual precipitation 2000-2010.**

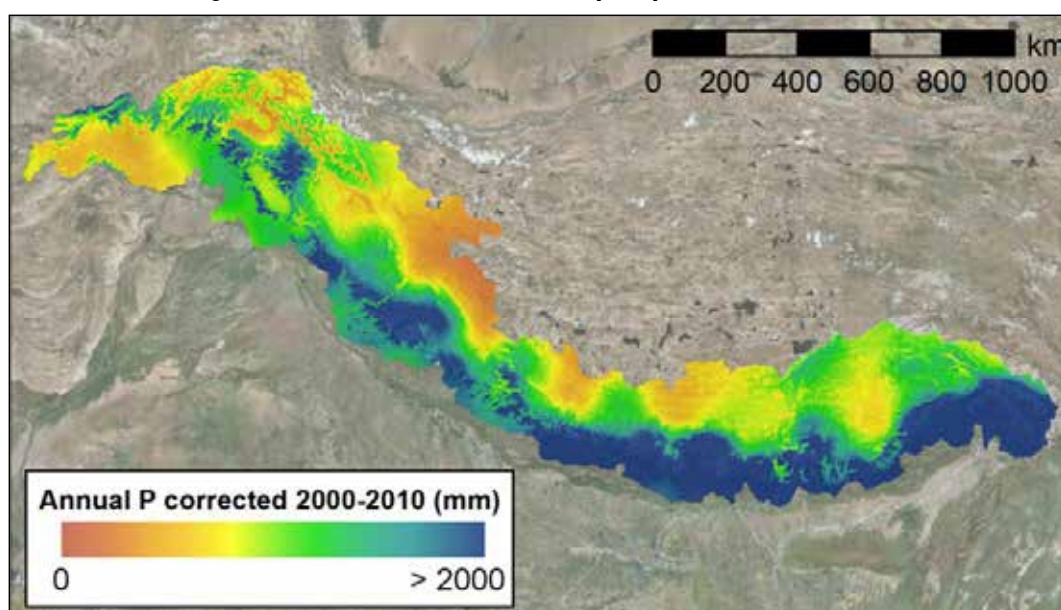
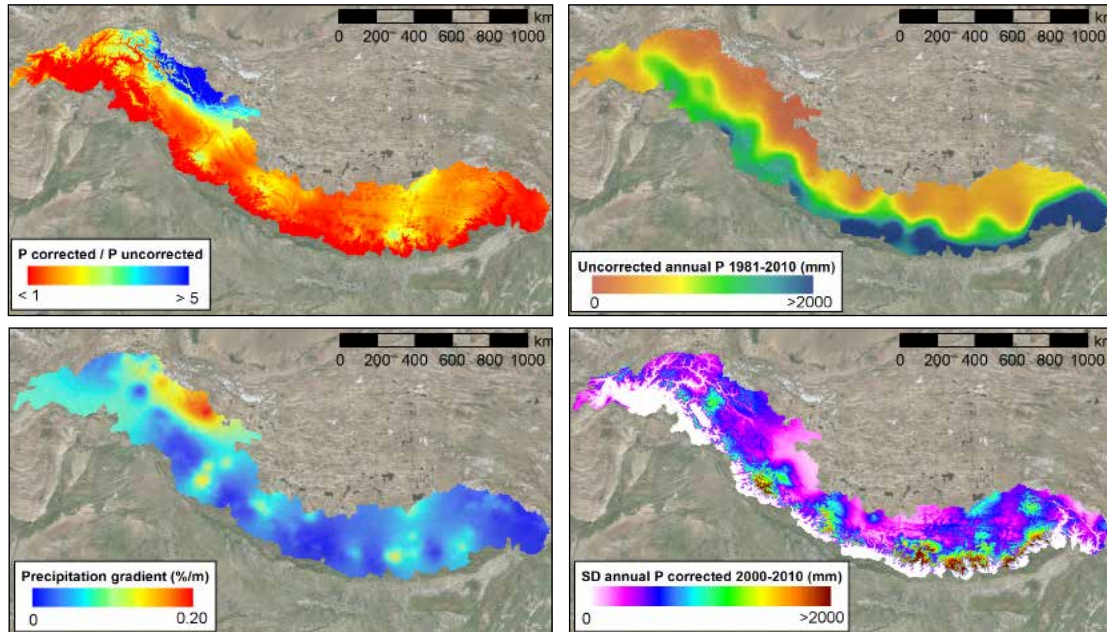


Table 7: **Parameter values used in precipitation correction model.**

Parameter	Acronym	Distribution	Mean	SD
Reference elevation (masl)	H <sub>REF</sub>	log-Gaussian	2500	500
Maximum elevation (masl)	H <sub>MAX</sub>	log-Gaussian	5500	500
Karakoram and Hindu Kush			4500	500
Other mountain ranges				
Degree day factor debris covered glacier (mm °C <sup>-1</sup> d <sup>-1</sup> )	DDFdc	log-Gaussian	7	2
Degree day factor debris free glacier (mm °C <sup>-1</sup> d <sup>-1</sup> )	DDFdf	log-Gaussian	2	2
Slope threshold (m m <sup>-1</sup> )	TS	log-Gaussian	0.2	0.05
Mass balance for individual glaciers	MB	Gaussian	Figure 12 (left)	Figure 12 (right)
Maximum annual ablation (m we yr <sup>-1</sup> )	AMAX	Gaussian	1.35	0.50

Figure 14: Annual uncorrected precipitation 2000-2010 (upper left). Standard deviation of corrected precipitation resulting from 100 realisations of Monte Carlo uncertainty analysis (upper right). Corrected precipitation divided over uncorrected precipitation 2001-2010 (lower left). Mean precipitation gradient (lower right).



### 3.3 Downstream climate

For the downstream parts of the IGB river basins, a more straightforward correction can be applied since the biases in the WFDEI dataset are much smaller there because of the higher station density and less complex climate. Air temperature data is downscaled from  $0.5^\circ \times 0.5^\circ$  ( $\sim 50 \times 50$  km) to  $10 \times 10$  km spatial resolution – similar what is done in the upstream domain by lapsing air temperature over the vertical difference between a DEM at  $10 \times 10$  km resolution and a DEM at  $0.5^\circ \times 0.5^\circ$ . A fixed vertical lapse rate ( $-0.0065 \text{ }^\circ\text{C m}^{-1}$ ) is applied. The precipitation fields in WFDEI which are already corrected to the GPCC are spatially interpolated from  $0.5^\circ \times 0.5^\circ$  ( $\sim 50 \times 50$  km), to  $10 \times 10$  km spatial resolution using a cubic spline interpolation.

# 4. Corrected Reference Climate Data

This chapter summarises the corrected reference climate datasets with figures illustrating the datasets' properties at the grid-cell level. Two datasets are delivered: one at 5x5 km spatial resolution for the upstream domain, and one at 10x10 km for the total domain. The 5x5 km upstream dataset is aggregated to a 10x10 km resolution and combined with the 10x10 km downstream data to generate the dataset for the total domain.

## 4.1 Upstream dataset

### 4.1.1 Air temperature

The corrected air temperature dataset is on average colder than the uncorrected data. The strongest negative corrections are made for the upper Indus basin and the upper Brahmapadura basin, whereas the corrections are mostly slightly positive or neutral for large parts of the upper Ganges basin.

Figure 15: **Corrected mean air temperature (1981-2010) upstream dataset.**

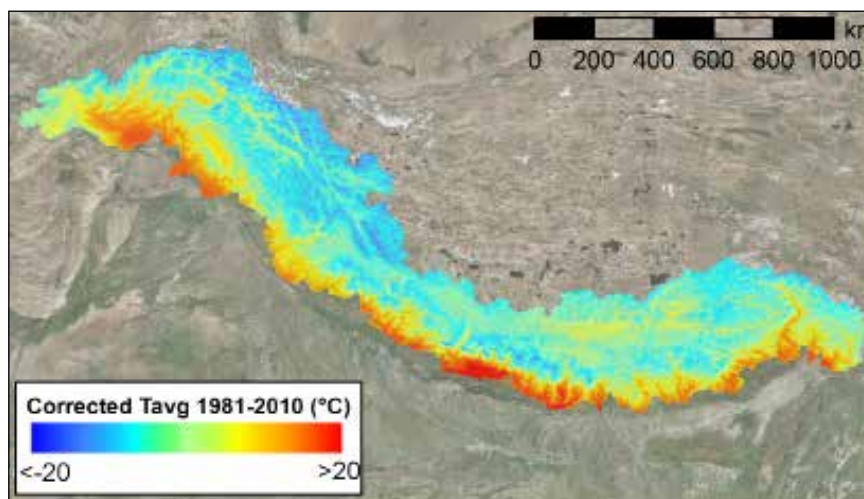
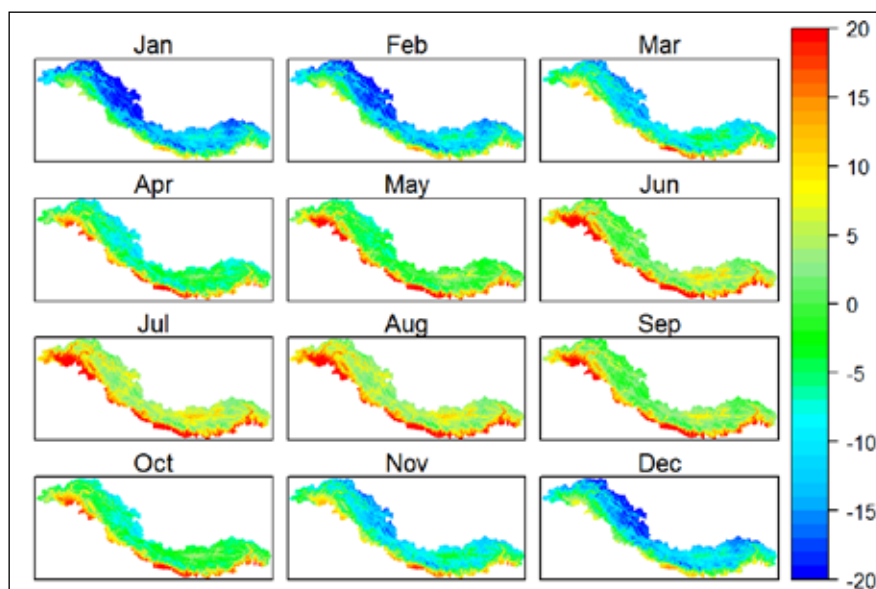


Figure 16: **Monthly mean air temperature (1981-2010) corrected upstream dataset.**



### 4.1.2 Precipitation

The strongest changes are present in the precipitation data, with the strongest corrections being made for the Indus basin, which indicates that the precipitation in the basin is being underestimated most severely in the uncorrected WFDEI dataset. The mean annual precipitation sum clearly shows the south to north and east to west gradients in the strength of the monsoon. Most of the precipitation falls on the southern and eastern ranges of the upstream domain. The intra-annual patterns in the data (Figure 18) show that the seasonal patterns are well captured in the dataset. Most of the precipitation falls during the monsoon season (June-September) on the southern and eastern ranges. Additionally, the changes in intensity of the monsoon during the monsoon season are well represented in the data. Precipitation in the most upstream parts of the Indus basin (Hindu Kush and Karakoram ranges) falls during the winter months, which is also well-represented in the data. This is nicely illustrated when looking at precipitation during the different seasons as percentages of the total annual precipitation (Figure 19). This clearly shows the southeast to northwest trend of decreasing monsoon dominance for the precipitation regime.

The correct representation of the fluctuations in precipitation intensity in space and time is of utmost importance for the forcing of hydrological models, for which the forcing data is often the most uncertain component in the modelling assessment for the HKH region.

Figure 17: **Corrected mean annual precipitation sum (1981-2010) upstream dataset and relative distribution of precipitation in north-south and west-east directions.**

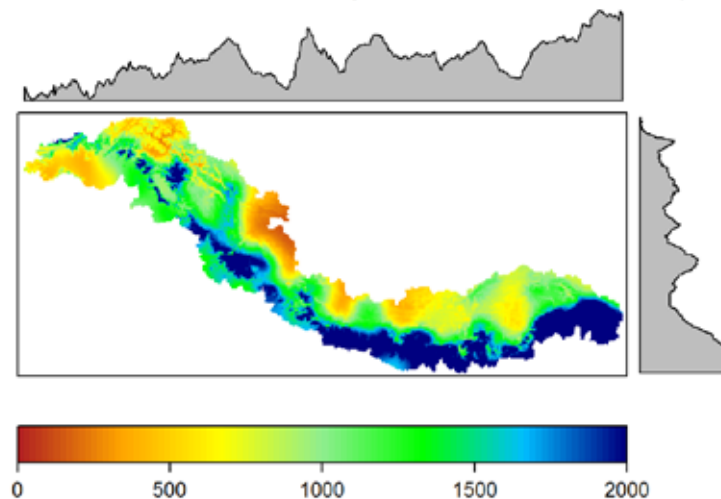


Figure 18: **Corrected mean monthly precipitation sum (1981-2010) upstream dataset.**

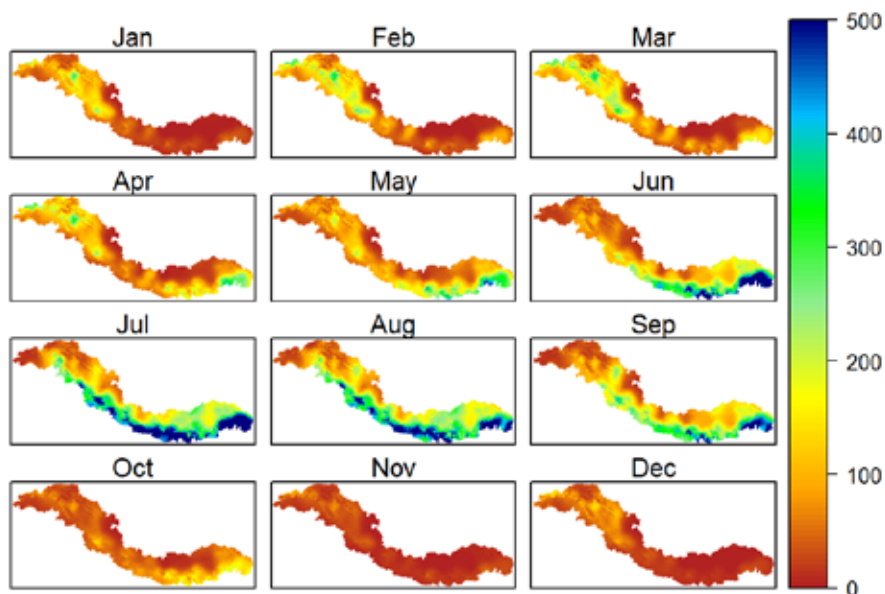
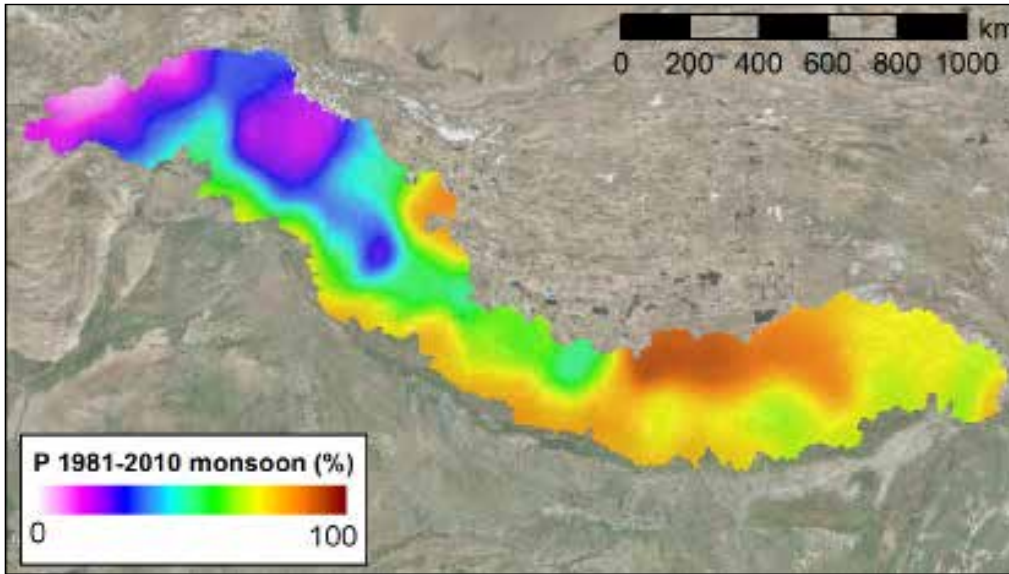


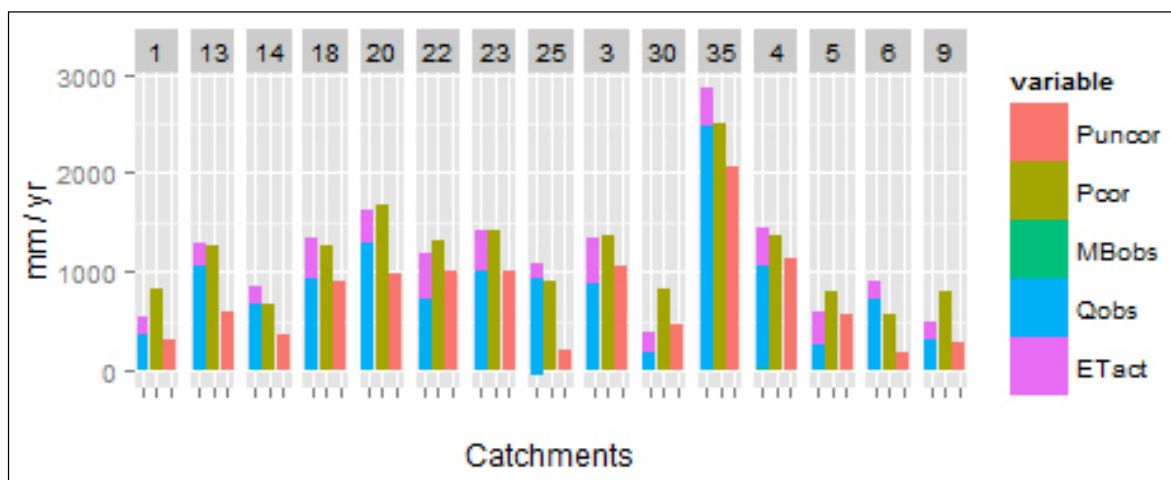
Figure 19: **Precipitation during the monsoon season (June–September) as a percentage of the total annual precipitation (left), and precipitation during winter (December–February) as a percentage of the total annual precipitation (right).**



*Validation to observed discharge and actual evapotranspiration*

The corrected precipitation dataset is subjected to a first order validation with other observed or estimated components of the water balance at the sub-basin level. It is assumed that the catchment’s corrected precipitation should equal the sum of the catchment’s discharge, actual evapotranspiration, and eventual increases in the water volume stored as glacier ice. When mass balance is negative, the decrease in the volume of water stored as ice is considered as outward flux. We estimate the average discharge from multiple multiyear discharge records. Note, however, that in all cases the period of the climatic dataset (1981-2010) and the period of the discharge records are only partly overlapping. Actual evapotranspiration is estimated from the PCR-GLOBWB model output for 2003-2007 [Wada *et al.*, 2011]. Glacier mass balance is estimated with the trends for 2000-2010 used in this study (Figure 12).

Figure 20: **Validation of corrected precipitation product for 15 sub-basins to observed discharge and estimated actual evapotranspiration.**



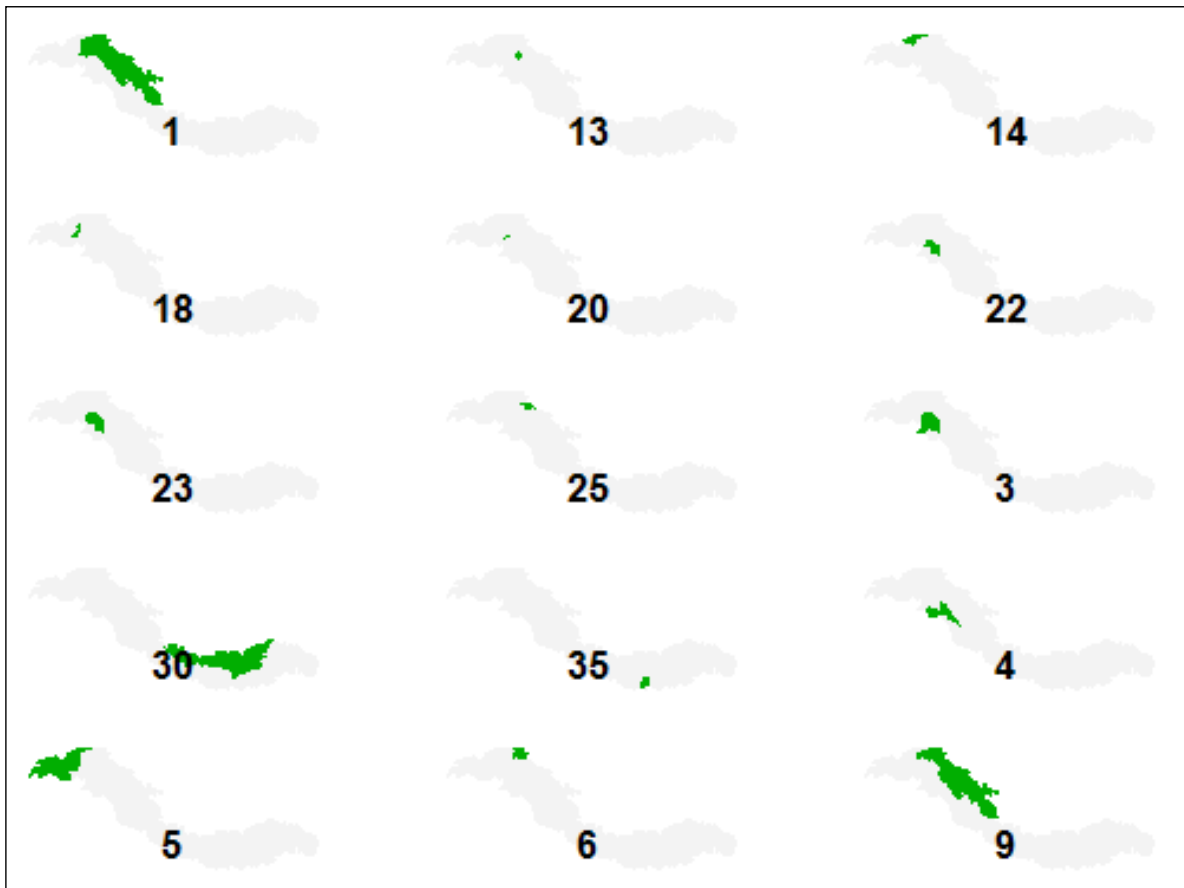


Figure 20 shows that, in most catchments, the uncorrected precipitation is by far not enough to have a closed water balance, whereas the water balance can be closed with the corrected precipitation data in most cases. This provides confidence that the corrected precipitation is close to reality in most cases, although there are cases where the corrected precipitation input is still too small (e.g. catchment IDs 6, 13, 18, 25, and 35). On the other hand, it seems that the corrected precipitation overestimates the precipitation on most northern parts of the basins, located on the Tibetan plateau (e.g. catchment IDs 9, and 30). However, an important remark to be made here is that fluxes such as infiltration into deep groundwater and sublimation, which can be significant in this area, are not included in this validation due to lack of observations. Besides, the comparison with fluxes that only overlap a part of the reference climate dataset means that this validation offers only a first-order estimate for the correctness of the data. Based on this validation exercise, we conclude that the corrected dataset is a significant improvement to the representation of precipitation in the upstream basins when compared with the uncorrected data.

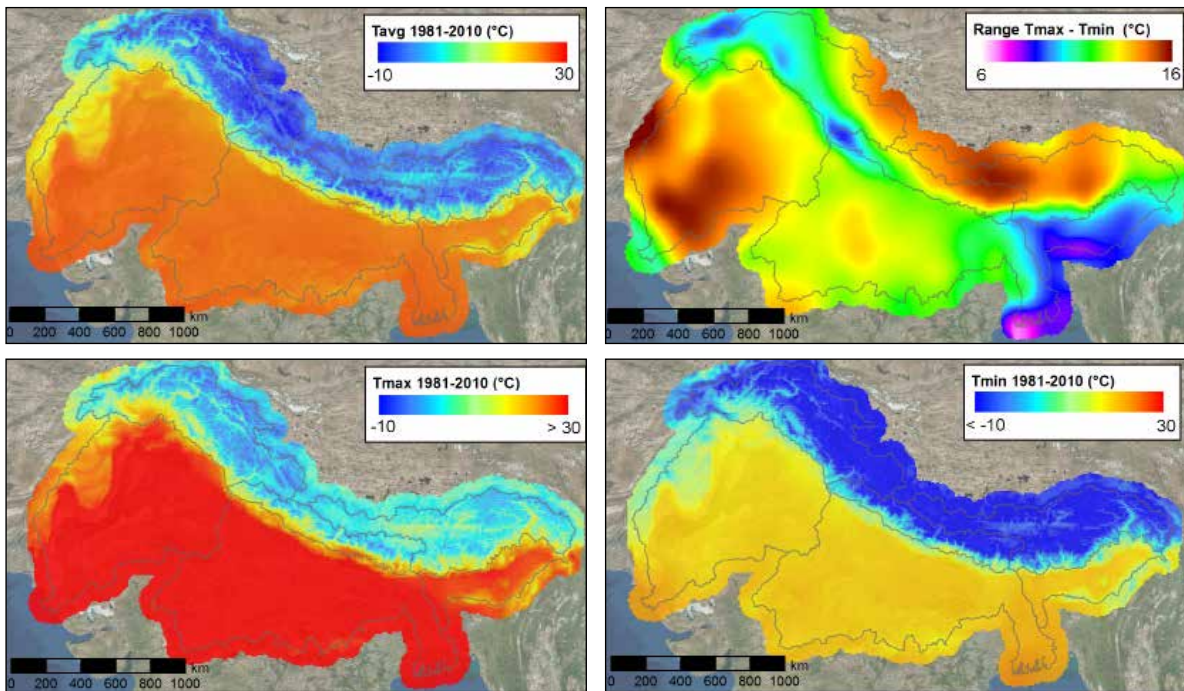
## 4.2 Total IGB domain

The dataset covering the entire Indus, Ganges, and Brahmaputra basins has a 10x10 km spatial resolution and contains the upstream dataset, which has been aggregated from a 5x5 km to 10x10 km spatial resolution. As visible in Figure 21 and Figure 23, the datasets are merged seamlessly and provide a consistent corrected dataset for the entire IGB domain.

### 4.2.1 Air temperature

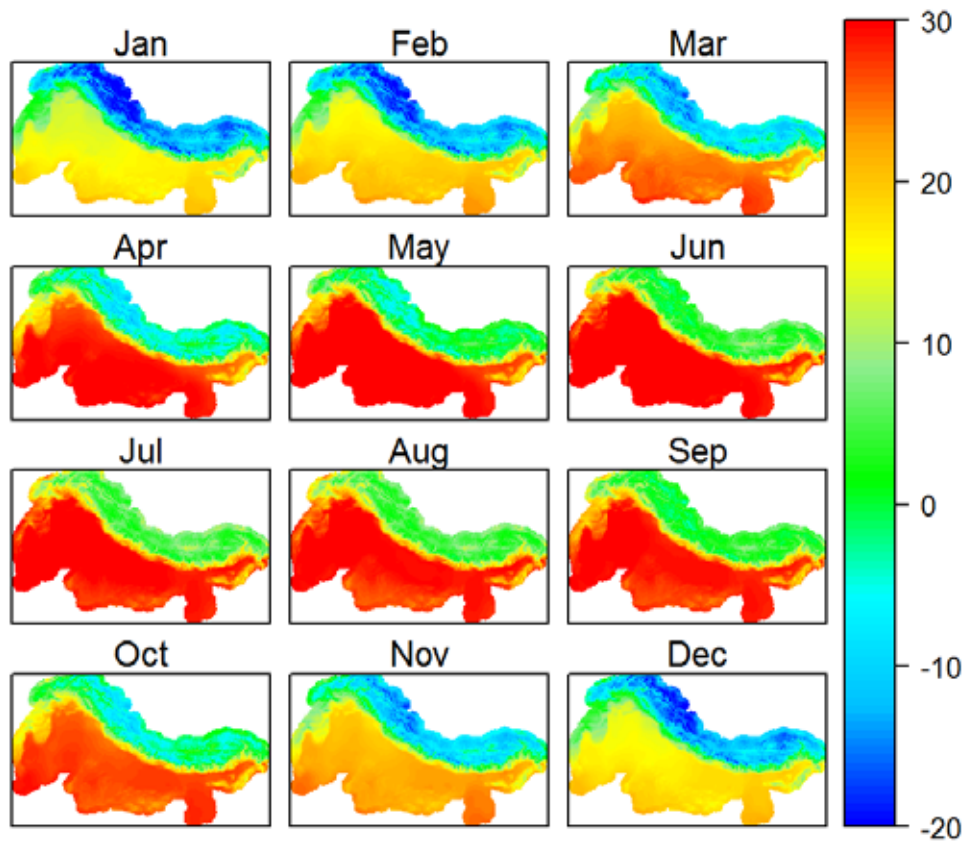
Figure 21 shows the mean temperature grids for the 30-year reference period. Means over the entire period are shown for mean air temperature, maximum air temperature, minimum air temperature and the diurnal range between the maximum air temperature, and the minimum air temperature. As expected, this diurnal range is largest for the driest regions: the lower Indus and the upstream parts located in the Tibetan plateau. The smallest ranges are seen in the wettest areas in the lower Brahmaputra basin (see Figure 23). This shows that the temperature and precipitation datasets are physically consistent.

Figure 21: Air temperature (1981-2010) corrected dataset covering entire IGB river basins: mean air temperature (upper left), range between maximum and minimum air temperature (upper right), maximum air temperature (lower left), and minimum air temperature (lower right).



The monthly averages of the mean air temperature (Figure 22) show the expected seasonal patterns with colder winters and warmer summers. Strong gradients are present with cold temperatures in the upstream parts of the basins and high temperatures in the downstream parts.

Figure 22: Corrected monthly mean air temperature (1981-2010) dataset covering the entire IGB river basins.



### 4.2.2 Precipitation

Figure 23 nicely illustrates the important effect that altitude has on precipitation patterns. The traverse from the Indo-Gangetic plain to the Himalayas, Karakoram, and Hindu Kush mountain ranges clearly shows the increasing precipitation with altitude. The spatial differences in precipitation quantities are clearly visible. South to north and east to west gradients in the intensity of the monsoon are well captured for the monsoon season (June-September, Figure 24). As mentioned before in section 4.1.2, the high-altitude winter precipitation in the upper Indus basin is also well represented in this corrected dataset.

Figure 23: **Mean annual precipitation sum (1981-2010) corrected dataset covering the entire IGB river basins.**

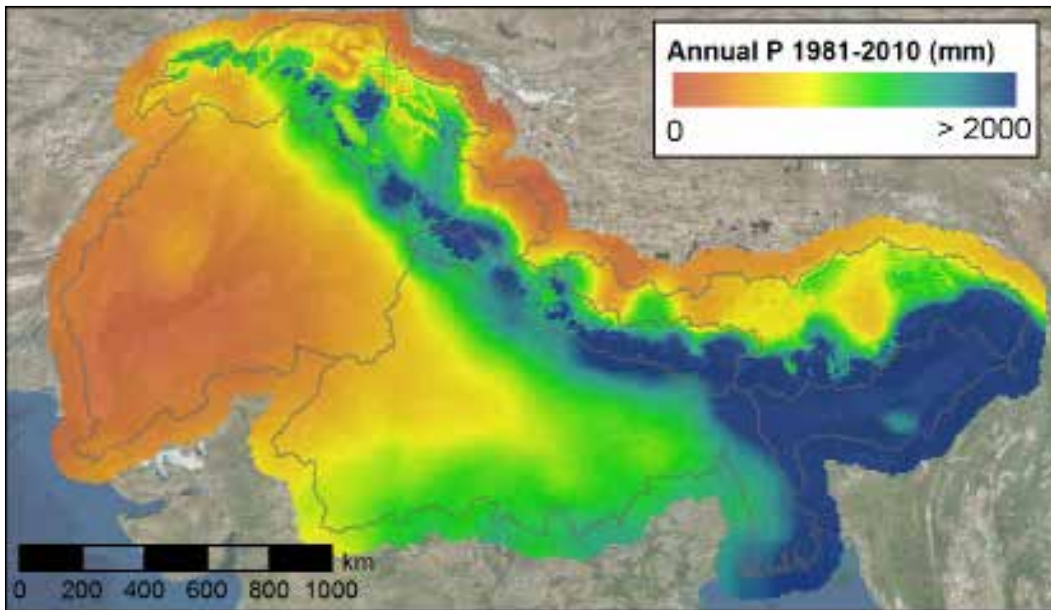
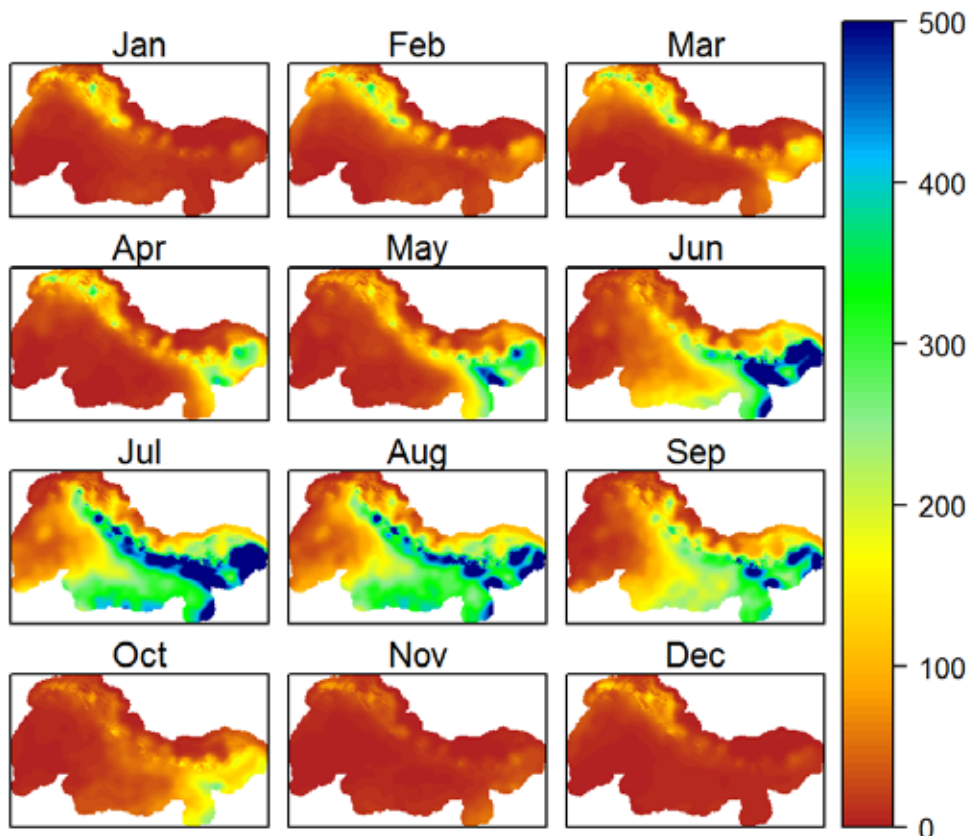


Figure 24: **Mean monthly precipitation sum (1981-2010) corrected dataset covering the entire IGB river basins.**



### 4.2.3 Reference evapotranspiration

The reference evapotranspiration ( $ET_{ref}$ ) is calculated for the total IGB at a 10x10 km spatial resolution and daily time step by applying the Modified-Hargreaves equation [Droogers and Allen, 2002]. The Modified-Hargreaves equation (MH-equation) has an advantage over the widely used Penman-Monteith equation in that it can be applied to low-data situations. The MH-equation requires extraterrestrial radiation, maximum air temperature, and minimum air temperature:

$$ET_{ref} = 0.0023 * 0.408 * Ra (T_{avg} + 17.8) * TD^{0.5}$$

where  $Ra$  ( $MJm^{-2} day^{-1}$ ) is the extraterrestrial radiation,  $T_{avg}$  ( $^{\circ}C$ ) the average daily air temperature, and  $TD$  ( $^{\circ}C$ ) the daily temperature range defined as the difference between the daily maximum and minimum air temperatures. The constant 0.408 is required to convert the units to mm, and  $Ra$  can be obtained from equations using the day of the year and the latitude of the grid cell. The reference evapotranspiration data is included in the upstream dataset as well as the downstream dataset.

Figure 25: Mean annual reference evapotranspiration (1981-2010).

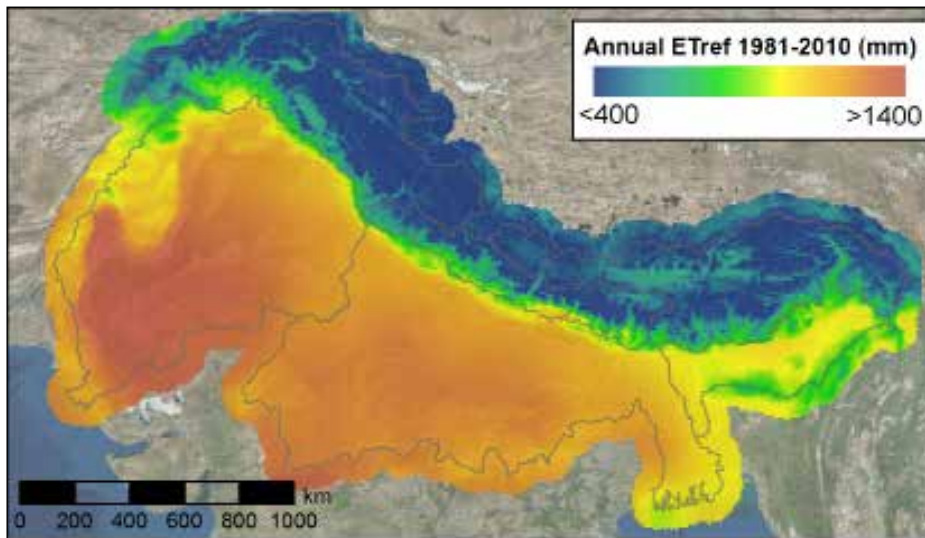
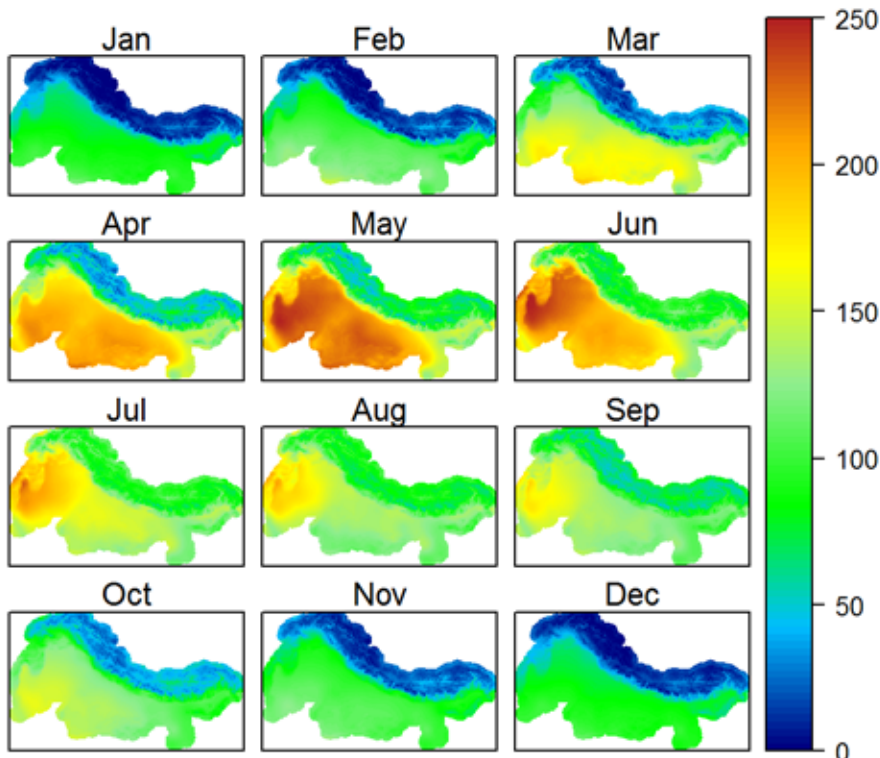


Figure 26: Monthly mean reference evapotranspiration (1981-2010).



### 4.3 Subregional summaries and trends in time

Table 8 shows the mean air temperature and mean annual precipitation for six subregions in the IGB domain, averaged over the entire reference period (1981-2010). The differences between the corrected data and the uncorrected data for the upstream basins are striking. Precipitation amounts are much higher (compare Table 3 and Table 8), with the largest correction being made for the upper Indus basin. Air temperatures have been corrected to cooler temperatures in the upstream basins.

**Table 8: Zonal averages of corrected climatic forcing per sub-basin.**

	Mean T 1981-2010 (°C)	Annual P 1981-2010 (mm)
Upper Indus	-1.6	1052
Lower Indus	23.8	373
Upper Ganges	2.4	1810
Lower Ganges	25.1	1139
Upper Brahmaputra	-1.1	1424
Lower Brahmaputra	21.8	2847

Mean air temperatures show increasing trends in all basins during the reference period (Figure 27). The dataset also captures the observed elevation dependent warming [Rangwala and Miller, 2012; Pepin et al., 2015], with steeper increasing trends for temperature in the upstream basins as compared to the downstream parts of the basins.

Linear regressions of precipitation trends show slightly decreasing or neutral trends for the subregions (Figure 28). These trends must be interpreted with care since the significance of these trends is questionable. Precipitation is characterised by a larger inter-annual variability, which makes it more difficult to infer significant trends.

**Figure 27: Zonal averages of annual mean air temperature (1981-2010) for the upstream basins (upper panel) and downstream basins (lower panel).**

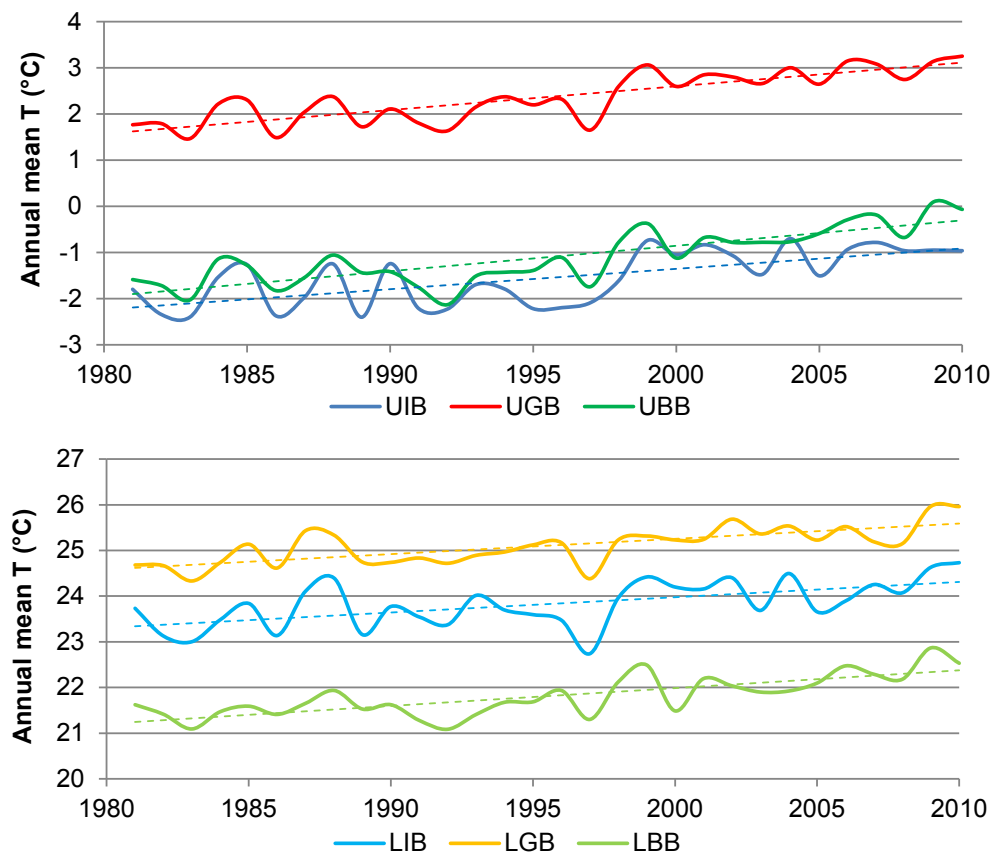
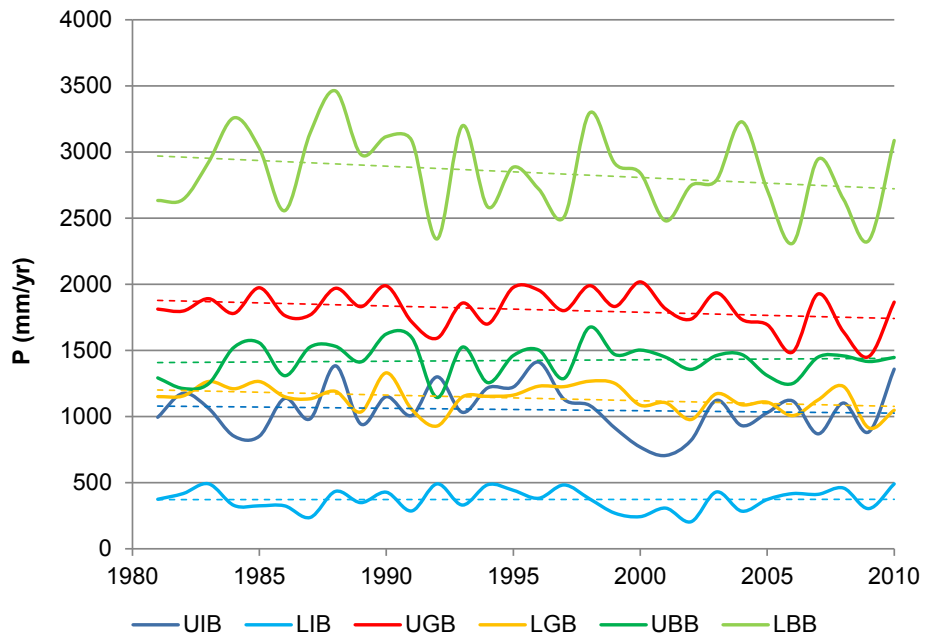


Figure 28: Zonal averages of annual precipitation sums (1981-2010).



# 5. Dataset Metadata

## 5.1 Upstream IGB dataset

<b>Projection</b>	WGS 84 UTM Zone 45N (EPSG:32645)		
<b>Extent</b>	xmin: -1330000 xmax: 1570000	ymin: 2940000 ymax: 419000	
<b>Spatial resolution</b>	5000 x 5000 meter (580 columns, 250 rows, 145000 grid cells)		
<b>Temporal resolution and timespan</b>	Daily time step, 1 Jan 1981 – 31 Dec 2010		
<b>Variables and units</b>	prec	Daily precipitation sum	mm
	tavg	Daily mean air temperature	°C
	tmax	Daily maximum air temperature	°C
	tmin	Daily minimum air temperature	°C
	eref	Reference evapotranspiration	mm
<b>Data format</b>	NetCDF (1 file per year and per variable)		
<b>Format of filenames</b>	HIAWARE_IGBupstr_variable_year.nc		

## 5.2 Total IGB dataset

<b>Projection</b>	WGS 84 UTM Zone 45N (EPSG:32645)		
<b>Extent</b>	xmin: -1600000 xmax: 1600000	ymin: 2300000 ymax: 420000	
<b>Spatial resolution</b>	10000 x 10000 meter (320 columns, 190 rows, 60800 grid cells)		
<b>Temporal resolution and timespan</b>	Daily time step, 1 Jan 1981 – 31 Dec 2010		
<b>Variables and units</b>	prec	Daily precipitation sum	mm
	tavg	Daily mean air temperature	°C
	tmax	Daily maximum air temperature	°C
	tmin	Daily minimum air temperature	°C
	eref	Reference evapotranspiration	5.2.1.1.1 mm
<b>Data format</b>	NetCDF (1 file per year and per variable)		
<b>Format of filenames</b>	HIAWARE_IGBtotal_variable_year.nc		

The dataset has a buffer around the basins to make resampling to coarser resolutions possible without losing parts of the basin in the resampled dataset.

# References

- Andermann, C; S. Bonnet; R. Gloaguen (2011) 'Evaluation of precipitation data sets along the Himalayan front'. *Geochemistry, Geophys. Geosystems*, 12(7), 1–16, doi:10.1029/2011GC003513.
- Bajracharya, SR; Shrestha, AB (2011), *The Status of Glaciers in the Hindu Kush-Himalayan Region*.
- "Batura Investigations Group" (1979), 'The Batura Glacier in the Karakoram Mountains and its variations'. *Sci. Sin.*, 22(8), 958–974.
- Dee, DP et al. (2011) 'The ERA-Interim reanalysis: configuration and performance of the data assimilation system', *Q. J. R. Meteorol. Soc.*, 137(656), 553–597, doi:10.1002/qj.828.
- Droogers, P, Allen, RG (2002) 'Estimating reference evapotranspiration under inaccurate data conditions', *Irrig. Drain. Syst.*, 16, 33–45.
- Duncan, JMA; Biggs, EM (2012), 'Assessing the accuracy and applied use of satellite-derived precipitation estimates over Nepal', *Appl. Geogr.*, 34, 626–638, doi:10.1016/j.apgeog.2012.04.001.
- Gardelle, J; Berthier, E; Arnaud, Y (2012) 'Slight mass gain of Karakoram glaciers in the early twenty-first century', *Nat. Geosci.*, 5(5), 322–325, doi:10.1038/ngeo1450.
- Gardelle, J; Berthier, E; Arnaud, Y; Kääb, a (2013) 'Region-wide glacier mass balances over the Pamir-Karakoram-Himalaya during 1999–2011', *Cryosph.*, 7(4), 1263–1286, doi:10.5194/tc-7-1263-2013.
- Harris, I; Jones, PD; Osborn, TJ; Lister, DH (2013) 'Updated high-resolution grids of monthly climatic observations' - the CRU TS3.10 Dataset, *Int. J. Climatol.*, doi:10.1002/joc.3711.
- Hewitt, K (2005) 'The Karakoram Anomaly? Glacier Expansion and the "Elevation Effect," Karakoram Himalaya', *Mt. Res. Dev.*, 25(4), 332 – 340.
- Hewitt, K (2007) 'Tributary glacier surges: an exceptional concentration at Panmah Glacier, Karakoram Himalaya', *J. Glaciol.*, 53(181), 181–188, doi:10.3189/172756507782202829.
- Hewitt, K (2011) 'Glacier Change, Concentration, and Elevation Effects in the Karakoram Himalaya, Upper Indus Basin', *Mt. Res. Dev.*, 31(3), 188–200, doi:10.1659/MRD-JOURNAL-D-11-00020.1.
- Huss, M (2013) 'Density assumptions for converting geodetic glacier volume change to mass change', *Cryosph.*, 7(3), 877–887, doi:10.5194/tc-7-877-2013.
- Immerzeel, WW; van Beek, LPH; Konz, M; Shrestha, AB; Bierkens, MFP (2011) 'Hydrological response to climate change in a glacierized catchment in the Himalayas', *Clim. Change*, 110, 721–736, doi:10.1007/s10584-011-0143-4.
- Immerzeel, WW; Pellicciotti, F; Shrestha, AB (2012) 'Glaciers as a Proxy to Quantify the Spatial Distribution of Precipitation in the Hunza Basin', *Mt. Res. Dev.*, 32(1), 30–38, doi:10.1659/MRD-JOURNAL-D-11-00097.1.
- Immerzeel, WW; Petersen, L; Ragettli, S; Pellicciotti, F (2014) 'The importance of observed gradients of air temperature and precipitation for modeling runoff from a glacierized watershed in the Nepalese Himalayas', *Water Resour. Res.*, 50, WR014506, doi:10.1002/2013WR014506.Received.
- Immerzeel, WW; Wanders, N; Lutz, AF; Shea, JM, Bierkens, MFP (2015) 'Reconciling high altitude precipitation with glacier mass balances and runoff', *Hydrol. Earth Syst. Sci.*, 12, 4755–4784, doi:10.5194/hessd-12-4755-2015.
- Kattel, DB; Yao, T; Yang, K; Tian, L; Yang, G; Joswiak, D (2012) 'Temperature lapse rate in complex mountain terrain on the southern slope of the central Himalayas', *Theor. Appl. Climatol.*, 113(3-4), 671–682, doi:10.1007/s00704-012-0816-6.
- Lutz, AF; Immerzeel, WW; Kraaijenbrink, PDA (2014) *Gridded Meteorological Datasets and Hydrological Modelling in the Upper Indus Basin. FutureWater Report 130*, Wageningen, The Netherlands.

- Maussion, F; Scherer, D; Mölg, T; Collier, E; Curio, J; Finkelnburg, R (2014) 'Precipitation Seasonality and Variability over the Tibetan Plateau as Resolved by the High Asia Reanalysis', *J. Clim.*, 27(5), 1910–1927, doi:10.1175/JCLI-D-13-00282.1.
- Palazzi, E; Von Hardenberg, J; Provenzale, A (2013) 'Precipitation in the Hindu-Kush Karakoram Himalaya: Observations and future scenarios', *J. Geophys. Res. Atmos.*, 118, 85–100, doi:10.1029/2012JD018697.
- Pepin, N; et al. (2015) 'Elevation-dependent warming in mountain regions of the world', *Nat. Clim. Chang.*, 5, 424–430, doi:10.1038/nclimate2563.
- Ragetti, S; Pellicciotti, F; Immerzeel, WW; Miles, E; Petersen, L; Heynen, M; Shea, JM; Stumm, D; Joshi, S; Shrestha, AB (2015) 'Unraveling the hydrology of a Himalayan watershed through integration of high resolution in-situ data and remote sensing with an advanced simulation model', *Adv. Water Resour.*, 78, 94–111, doi:10.1016/j.advwatres.2015.01.013.
- Rangwala, I; Miller, JR (2012) 'Climate change in mountains: A review of elevation-dependent warming and its possible causes', *Clim. Change*, 114, 527–547, doi:10.1007/s10584-012-0419-3.
- Schneider, U; Becker, A; Finger, P; Meyer-Christoffer, A; Ziese, M; Rudolf, B (2013) 'GPCC's new land surface precipitation climatology based on quality-controlled in situ data and its role in quantifying the global water cycle', *Theor. Appl. Climatol.*, 26, doi:10.1007/s00704-013-0860-x.
- Terink, W; Lutz, AF; Simons, GWH; Immerzeel, WW; Droogers P (2015) 'SPHY v2.0: Spatial Processes in Hydrology', *Geosci. Model Dev.*, 8, 2009–2034, doi:10.5194/gmd-8-2009-2015.
- Wada, Y; van Beek, LPH; Bierkens, MFP (2011) 'Modelling global water stress of the recent past: on the relative importance of trends in water demand and climate variability', *Hydrol. Earth Syst. Sci.*, 15(12), 3785–3808, doi:10.5194/hess-15-3785-2011.
- Weedon, GP; Gomes, S; Viterbo, P; Shuttleworth, WJ; Blyth, E; Österle, H; Adam, JC; Bellouin, N; Boucher, O; Best, M (2011) 'Creation of the WATCH Forcing Data and Its Use to Assess Global and Regional Reference Crop Evaporation over Land during the Twentieth Century', *J. Hydrometeorol.*, 12(5), 823–848, doi:10.1175/2011JHM1369.1.
- Weedon, GP; Balsamo, G; Bellouin, N; Gomes, S; Best, MJ; Viterbo, P (2014) 'The WFDEI meteorological forcing data set: WATCH Forcing Data methodology applied to ERA-Interim reanalysis data', *Water Resour. Res.*, 7505–7514, doi:10.1002/2014WR015638. Received.
- Winiger, M; Gumpert, M; Yamout, H (2005) 'Karakorum-Hindukush-western Himalaya: assessing high-altitude water resources', *Hydrol. Process.*, 19(12), 2329–2338, doi:10.1002/hyp.5887.

© HI-AWARE 2016  
Himalayan Adaptation, Water and Resilience (HI-AWARE)  
c/o ICIMOD  
GPO Box 3226, Kathmandu, Nepal  
Tel +977 1 5003222 Email: [hi-aware@icimod.org](mailto:hi-aware@icimod.org)  
Web: [www.hi-aware.org](http://www.hi-aware.org)

ISBN 978 92 9115 420 3